ITA MAI TAI GUYOT: A

COMPARATIVE GEOPHYSICAL STUDY

OF WESTERN PACIFIC SEAMOUNTS

A THESIS SUBMITTED TO THE GRADUATE DIVISION OF THE
UNIVERSITY OF HAWAII IN PARTIAL FULFILLMENT
OF THE REQUIREMENTS FOR THE DEGREE OF

MASTER OF SCIENCE

IN GEOLOGY AND GEOPHYSICS

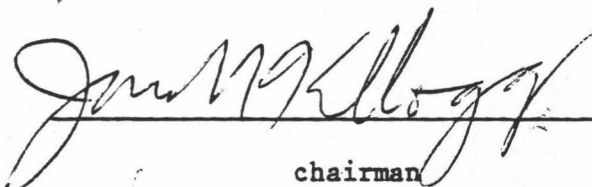DECEMBER 1985

By

Bruce Steven Wedgeworth

Thesis Committee:

James N. Kellogg, Chairman
Loren W. Kroenke
Eduard Berg

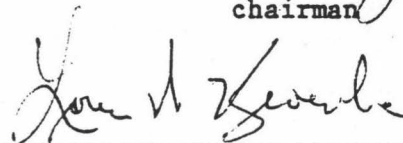We certify that we have read this thesis and that, in our opinion, it is satisfactory in scope and quality as a thesis for the degree of Master of Science in Geology and Geophysics.

THESIS COMMITTEE

_____
chairman

_____

_____

ACKNOWLEDGEMENTS

Rowland, John and JoAnn Sinton, Adam Weiner, Kathy Yamauchi, and Rob Yonover.

Very special thanks to my parents who never waivered in their love and support, who gave me the courage to make it my own way, and who, with me, never gave up.

ABSTRACT

Ita Mai Tai is a large, uncompensated seamount on the eastern edge of the East Mariana Basin. A large positive gravity anomaly of 254 mgal characterizes the summit and a low of -69 mgal, the surrounding moat. Using polygonal prisms to approximate the bathymetry, the observed gravity was inverted to calculate an average density of 2.59 g/cm^3 for the seamount. Other geologic data and seismic reflection profiles from DSDP Legs 20 and 89 provided further modeling constraints such as the density of the volcanic conduit and the density of sediment bodies. The drill sites describe a volcanic edifice formed in the Aptian/Albian on Jurassic/Cretaceous crust. The volcanism is recorded in volcanoclastic and epiclastic deposits in the basins nearby. The guyot was covered initially by a succession of reefal and lagoonal sediments followed by a thick mantling of pelagic sediments after it subsided.

Seismic reflection records indicate two different depths to basement on either side of Ita Mai Tai which may be explained by eruptions along or near an unrecognized fossil plate boundary. Gravity models that adequately match the calculated and observed data sets for Ita Mai Tai show little crustal thickening, suggesting that Ita Mai Tai is almost completely uncompensated isostatically. A study of ninety-six other western Pacific seamounts including Sio Guyot, a completely compensated seamount in the Mid-Pacific Mountains, show a linear inverse relationship between the maximum free-air anomaly and the minimum depths to the tops of seamounts, approximated by $g_z = (3800m - z) / 16.0$. Ita Mai Tai and Sio Guyot are seen as end members with their contrasting degree of compensation. To determine whether the observed anomalies could be explained by crustal "roots", theoretical models at 0 and 100

percent local compensation were derived for all western Pacific seamounts studied. Most of the observed gravity anomalies for seamounts in this study lie in the field between the theoretical lines of 0 and 100 percent compensation. Twenty-two appear to be more than 100 percent compensated.

A map of isostatic compensation shows a distinct break between the eastern and western Marshall Islands, perhaps indicating different ages of seamount formation. There is as much as a 200 mgal difference in the gravity field observed for well-surveyed seamounts and islands of the same size in the western Pacific. The sea floor age at the time of seamount formation seems to vary inversely with the relative amount of compensation. The over-compensated seamounts may have been erupted near Cretaceous ridge crests rather than in a mid-plate event as has been previously thought.

TABLE OF CONTENTS

LIST OF TABLES

LIST OF ILLUSTRATIONS

INTRODUCTION

A major goal in the application of the theory of plate tectonics in the Pacific has been determining the age and location of the oldest part of the Pacific plate. An attempt to reach this objective was made in 1971 when DSDP Leg 20 drilled Site 199 in the East Mariana Basin (Fig. 1). It was anticipated that Jurassic lithosphere would be encountered [Larson, 1976; Hilde et al., 1977; Shipley et al., 1983; and others]. Unfortunately, deep water drilling difficulties prevented this primary objective from being reached, and an alternate site was chosen farther east in a cluster of shallow seamounts between the Magellan and Marshall seamount chains (Fig. 1). Three holes were drilled at Sites 200, 201 and 202 on one of these seamounts located at $12°45'N$, $156°45'E$ (Fig. 2). This seamount was given the informal name Ita Mai Tai Guyot by Bruce Heezen which means "no damn good" in Tahitian [M. Tharp, pers. comm., 1984], possibly because basement was not reached. A second unsuccessful attempt to reach Jurassic basement was made in 1982 when DSDP Leg 89 drilled Site 585 just north of Ita Mai Tai. Other cruises across Ita Mai Tai include those of Conrad 1205, DDM05 in 1971 and Vema 3401 in 1977.

In 1981 the Hawaii Institute of Geophysics research vessel Kana Keoki surveyed Ita Mai Tai (Fig. 2) and other charted and uncharted seamounts in the central and western Pacific collecting bathymetric, gravimetric, magnetic, petrologic and seismic reflection profiling data. Although magnetic data also were obtained, the magnetic field appears too chaotic to attempt to model [W. Sager, pers. comm., 1984].

Figure 1. Bathymetric and tectonic map of the North Pacific
Ocean (AAPG, Circum-Pacific Series, 1981).

3
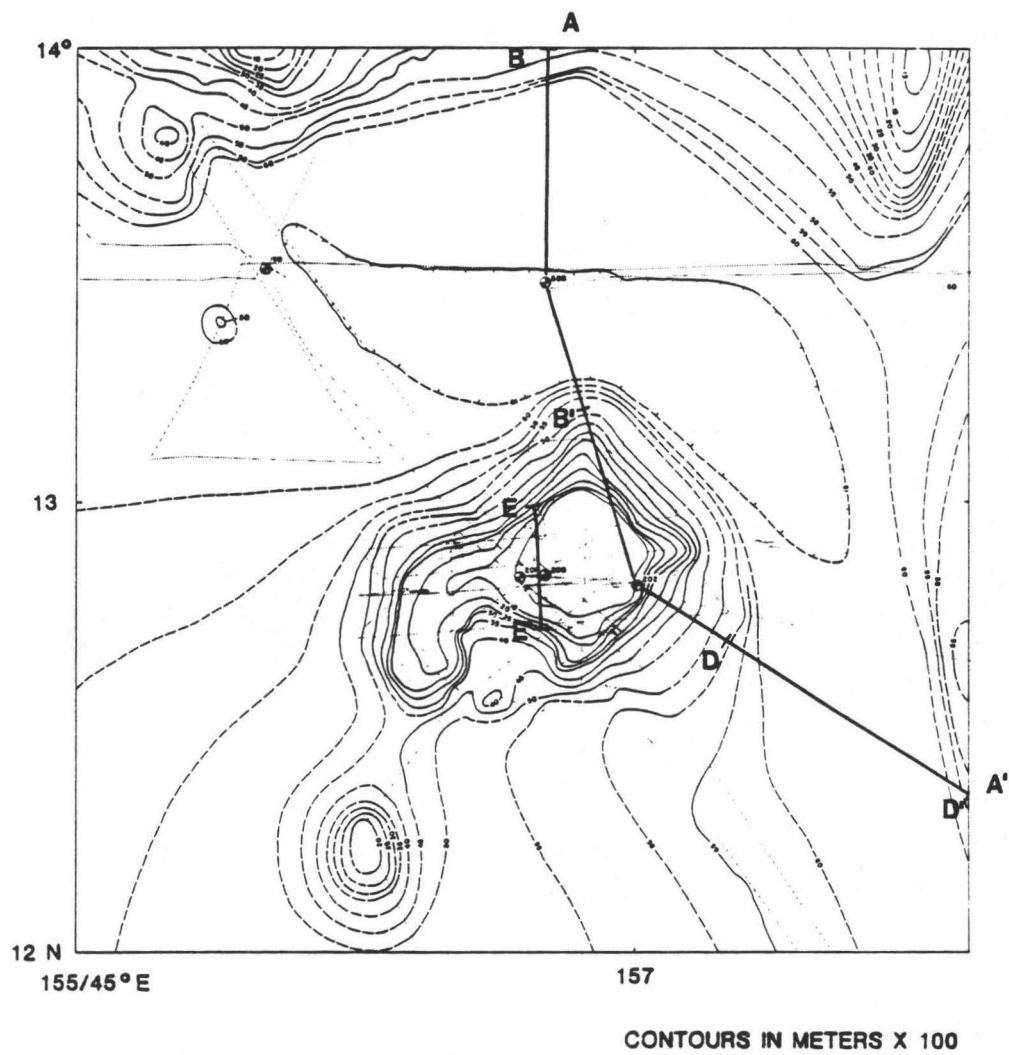
Figure 2. Bathymetry of Ita Mai Tai Guyot. Track lines are
indicated by dotted lines. Seismic cross-
sections and DSDP sites are also indicated.

The purpose of this study is to compile and analyze the additional geophysical data to determine the crustal structure of Ita Mai Tai, its degree of isostatic compensation, and its tectonic history. In order to construct accurate models it was necessary to have as much information as possible on the bathymetry, sediment distribution, geology, density distribution and gravity of Ita Mai Tai. Therefore, these topics will be discussed before the section on model studies. The results of this study also prompted a comparative investigation of other Pacific seamounts and islands to see if trends in regional compensation could be detected that might give clues to the origin of western Pacific seamounts.

REGIONAL FRAMEWORK

There is a striking dichotomy in morphology and structure between the Eastern Pacific and the Western Pacific, (Fig. 1). The picture in the Eastern Pacific seems relatively simple. The sea floor there is characterized by linear island chains with straightforward age progressions, large fracture zones, and simple magnetic lineations. By contrast, the sea floor in the western Pacific is a complicated collection of large clusters of seamounts and oceanic plateaus.

There have been several hypotheses advanced to explain the distribution of these western Pacific seamounts. The Wilson-Morgan "hotspot" hypothesis for the origin of seamounts predicts linear chains with a progressive age of formation. A second hypothesis is that there was a period of mid-plate volcanism in the Cretaceous

during which a widespread area of the western Pacific lithosphere was thinned by a large thermal event [Menard 1964, Schlanger and Premoli-Silva, 1981; Menard, 1984]. Seamounts formed by this mechanism would be expected to show a random distribution, simultaneous regional uplift, and variable paleolatitudes of formation. A third hypothesis is that these seamounts were formed near ridge crests and transform faults. The first and third hypotheses are not necessarily mutually exclusive. (Iceland, the Galapagos and the Mid-Pacific Mountains are possible examples of both mechanisms at work). Seamounts formed near ridge crests should have ages similar to the age of the crust on which they were erupted, a topography reflecting a rectilinear character, and be locally compensated.

Ita Mai Tai, a typical western Pacific seamount, is located on the eastern side of the Mariana Basin. The East Mariana Basin is bordered by the Magellan Seamounts to the north, the Marshall Islands to the east, the Caroline Islands to the south, and the Mariana Trench to the west. The basin is also quite far from well defined magnetic anomaly lineations. The Japanese magnetic lineations are 1500 km to the northwest, the Hawaiian magnetic lineations are about 1000 km to the northeast, the Nauru lineations are almost 1000 km to the southeast, and the Phoenix magnetic lineations more than 1500 km to the east-southeast (Fig. 1). The region between these lineations including the East Mariana Basin is characterized by low amplitude or ambiguous magnetic lineations usually referred to as the Jurassic Magnetic Quiet Zone which makes determining the age of sea floor near Ita Mai Tai a problem.

Shipley et al., (1983) assumed a spreading rate of 4.7 cm/yr and extrapolated from M-25 in the Phoenix lineations to estimate the age of the crust in the East Mariana Basin. Paleomagnetic data from sites 585, 289, and 462 indicate that the western Central Pacific had 4.5 cm/yr of northward drift between the Aptian and Campanian [Scientific Party, Leg 89, 1983]. Other authors have also concluded that the oldest oceanic crust in this part of the Western Pacific is Jurassic [Larson and Chase, 1972; Hilde et al., 1976]. However, Kroenke, in Hilde et al., (1977), has suggested that there was an episode of generally north-south intra-plate spreading starting 110 Ma and that the crust presently beneath the East Mariana Basin is upper Cretaceous. The lowest section of Site 585 encountered late Aptian hyaloclastite-rich turbidite and debris flows from the surrounding subaerial volcanoes. This site stopped just short of sampling the oceanic basement, and thus there is still no direct evidence for the age of the basin.

SEAMOUNT MORPHOLOGY

The bathymetric map of Ita Mai Tai Guyot is shown in Figure 2. Ita Mai Tai rises 4700 m from abyssal depths around 6000 m to a minimum depth of 1402 m. The height is considerably greater than the average relief of 1 km found for a survey of 6530 Pacific seamounts [Udintsev and others, 1976]. The shape of the seamount is subconical. An 'L' shaped flank ridge extends to the west and turns to the south toward other seamounts in the chain. The basal diameter measures

approximately 90 km and covers some 6400 km^2 (see Appendix A for volume calculations), which is much greater than the mean of north Pacific volcanoes [Batiza, 1982].

The summit area is quite uniform and flat. A break in slope occurs at about 2200 m below which the slope of the upper flanks is as steep as 35°. Gradually the slope decreases to average 9-10° on the lower flanks, a value comparable with that of subaerial volcanoes [Lonsdale and Spiess, 1977]. The northern and eastern flanks are bordered by a shallow depression or moat as outlined by the 6100 m contour.

SEDIMENTARY BASIN STRATIGRAPHY

The shapes and depths of the sediment filled basins to the north and southeast (Profiles A, B and D) were determined from HIG and DSDP Leg 89 airgun seismic reflection records (Appendix B). The shapes and depths of the pelagic cap units (Profile E) and the northern basin (Profile C) were determined from HIG airgun seismic reflection records. The locations of those profiles selected for this study are shown in Figure 2.

Profile A-A´ (Fig. 3) is a complete transect of Ita Mai Tai from north to southeast. It includes a seamount farther north, a deep sediment filled basin to the north, and another basin to the southeast. The most interesting aspect of this profile is the apparent difference in the depths to acoustic basement in the two basins. The northern basin appears to be much deeper than the

southeast basin. The difference in depth is an important factor in controlling the gravity modeling of Ita Mai Tai and will be discussed in more detail below in Figures 9 and 11.

Profile B-B´ (Fig. 4) completely crosses the northern basin shown on Figure 3. The basin is approximately 73 km wide at this point and the sea floor is 6100 m deep. DSDP Site 585 is located about midpoint. The two-way travel-time through the sediments to the floor of the basin is approximately one full second. Five lithologic units in the drilling record are depicted and labeled in the figure. The velocity of each of the lithologic units, their travel-times and maximum thicknesses, are based on closely spaced velocity and density measurements from the drilling record of Site 585 [Scientific Party, Leg 89, 1983] and are shown in Table I.
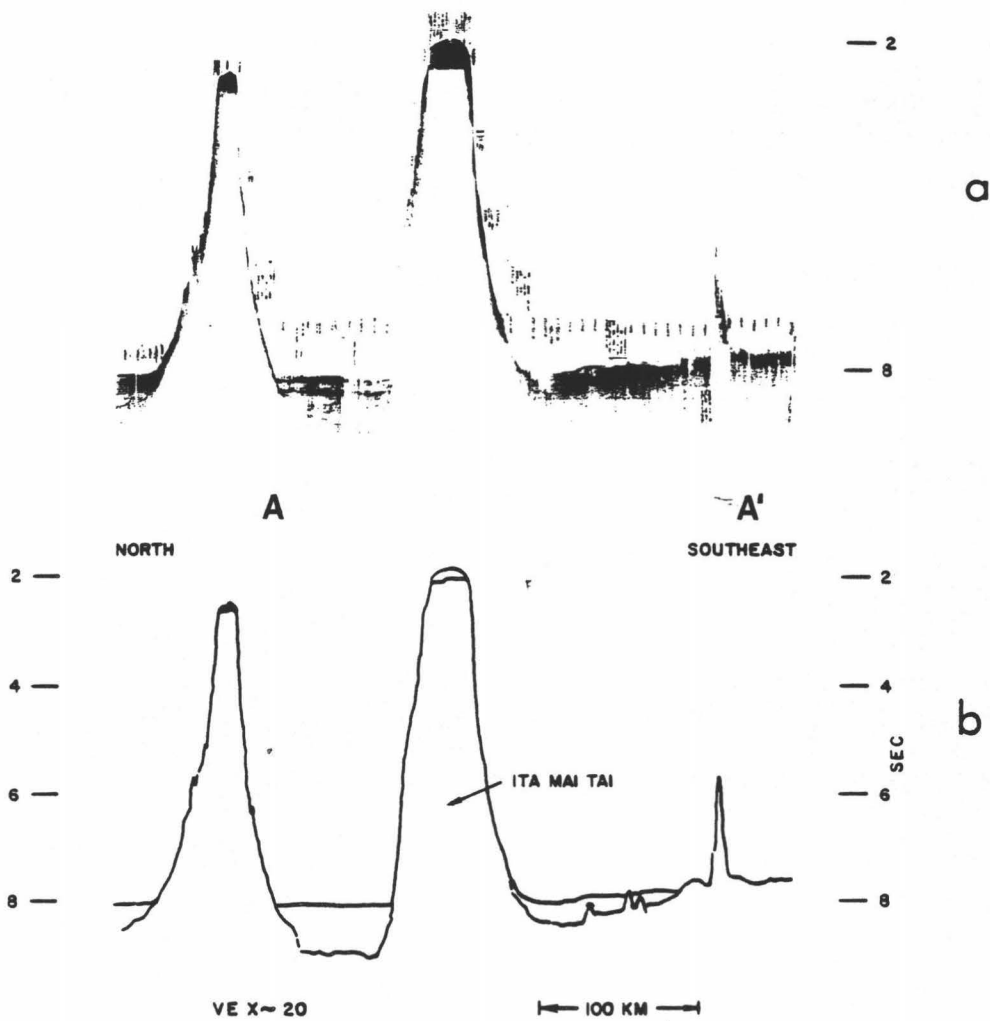
Figure 3. (a) Photo of airgun seismic reflection record across Ita Mai Tai during DSDP Leg 89 crossing. (b) Line drawing showing the basin depths on either side of Ita Mai Tai. See Figure 2 for location of transect.

Figure 4.   Photo of airgun seismic reflection record of
            basin to the north of Ita Mai Tai (Glomar Challenger,
            Leg 89 profile). (b) Line drawing showing units and
            from Site 585 drilling record, and locations of lava
            flows and sills.

TABLE I

DSDP LEG 89, SITE 585 DRILLING RECORD

	Velocity (km/s)	Travel-time (s)	Maximum Thickness (m)
Unit I Clay, nannofossil ooze Pleistocene	1.50	0.17	256
Unit II Nannofossil chalk, zeolitic claystone M. Eocene-Maas.	1.89	0.08	143
Units III + IV Zeolitic claystone, chert Maas.-Campanian	2.01	0.04	86
Unit V Zeolitic claystone, radiolarian siltstone Campanian-M. Albian	2.01	0.05	105
Unit VI Volcaniclastic debris M. Albian-L. Aptian	2.18-3.2	0.09-0.14	303

The unit thicknesses were independently estimated from HIG airgun seismic reflection records over the northern basin (Appendix B). Acoustic basement begins at about 9 seconds of two-way traveltime or 6900 m. The sediments in the basin are about 900 m thick. The thickest layer, a section containing volcaniclastic turbidites and debris flows (Unit VI), is also the lowest (Fig. 4). There is an especially strong reflector near 8.4 seconds that extends all the way across the section. This has been interpreted as the top of Unit II, where a large density contrast of 0.4 gm/cm^3 is encountered between recent clays and oozes and the Eocene chalks, limestones, cherts and ash beds.

Other aspects to consider are what are interpreted to be lava flows and sills close to Ita Mai Tai between 8.3 and 8.4 seconds. Similar flows have been described for the Ontong Java Plateau by Stoeser (1975) and Kroenke (1972). The flows and sills appear as bright reflectors which tend to obscure details below them (Fig. 4). If the sills in Unit II originated from Ita Mai Tai then the edifice must have been active during the deposition of Unit II. Unit VI is interpreted by the author to be the main edifice building deposit because it is composed of volcanogenic sediments. The layer that lies on top of Unit II at Site 585 has also been interpreted as volcanogenic in origin, probably from other seamounts such as the one to the north.

Profile D-D' (Fig. 5) crosses the southeast basin. The width of the basin along track is approximately 100 km. This basin appears to be much shallower than the other, only extending to 8.4 seconds or
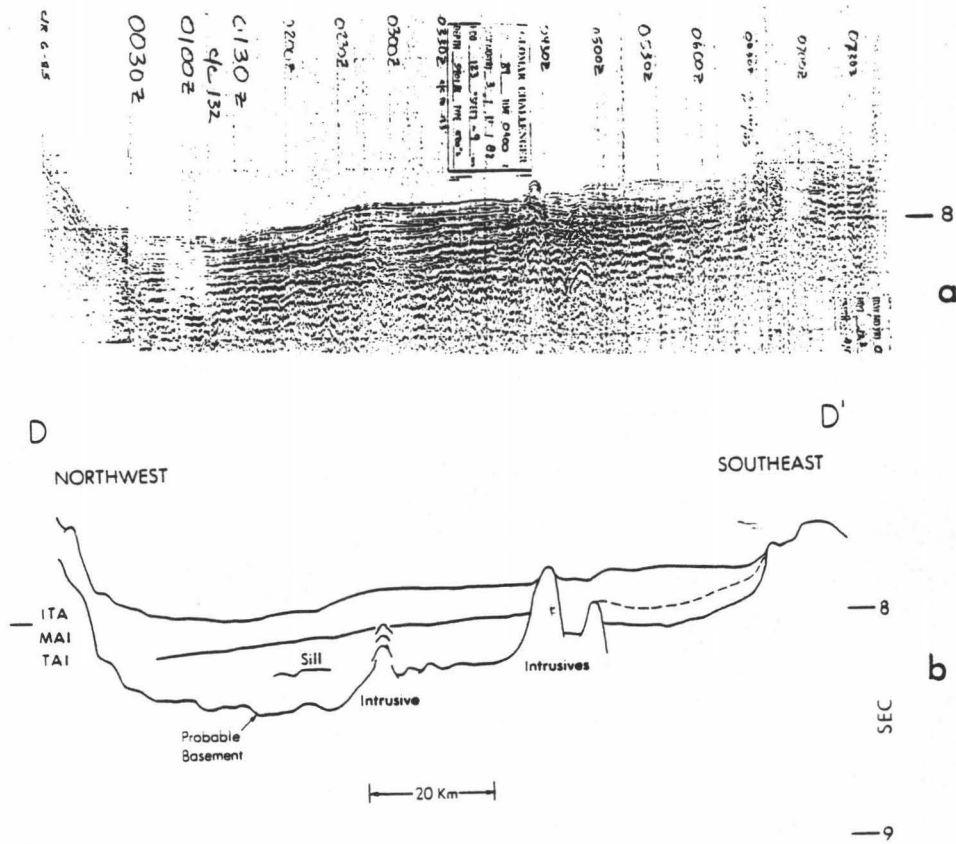
Figure 5. Photo of airgun seismic reflection record of
basin to the southeast of Ita Mai Tai (Glomar
Challenger, Leg 89 profile). (b) Line drawing
showing the probable depth to basement, and
locations of intrusive-structures.

about 6300 m. Total sediment thickness contained in the southeast basin is about 300 m as opposed to 900 m in the northern basin. Again, there is evidence for sills near 8.3 seconds. However, these, and the bright reflector extending across the basin between 8.1 and 8.2 seconds of reflection time, may be obscuring the depth to true basement. Models for these scenarios are described in a following section. Several diapiric or piercement structures extend upward from the basement. One, in fact, stands above the surrounding sediments on the sea floor. These may be intrusive volcaniform features related to the formation of the other seamounts in the vicinity. Their ages are unknown but are probably late Cretaceous because the radiometric age determinations of three other nearby seamounts (Scripps, Lamont, and Wilde) are all late Cretaceous [Ozima et al., 1977].

EDIFICE STRUCTURE

Profile E-E´ (Fig. 6) traverses the western end of the summit area north to south. DSDP holes 200 and 201 lie just to the east and west of this profile (Fig. 2). There are four different acoustic layers or strata present (Fig. 6). The smooth and continuous uppermost layer is the pelagic cap which drapes the entire top of the structure except for the northernmost end and is thickest in the middle part of the profile. There is little or no sediment evident on the flanks. The second layer is a thin but bright reflector interpreted as hard oolitic limestone. This layer is sporadically distributed, apparently occuring only where the pelagic sediments are
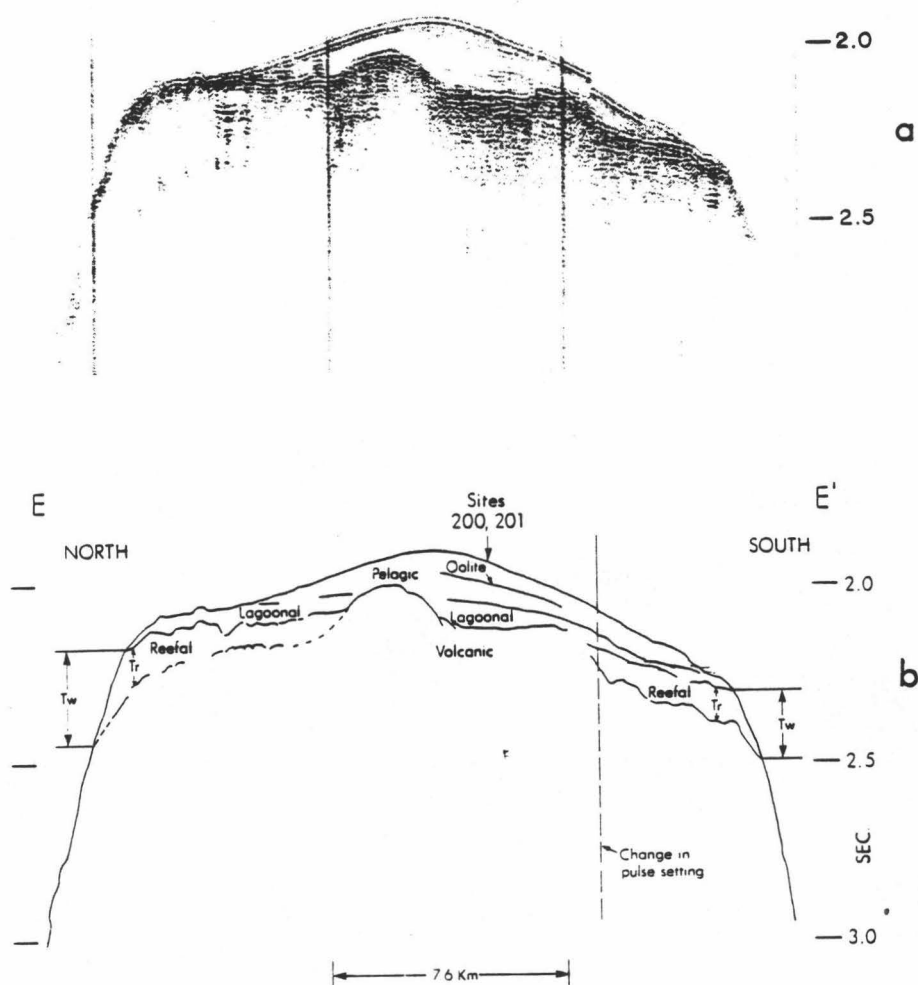
Figure 6. (a) Photo of airgun EPC seismic reflection record from KK810626 Leg 2 over the summit of Ita Mai Tai. (b) Line drawing showing the components of the pelagic cap. This transect lies between DSDP Sites 200 and 201 (Figure 2). T_w is the two way travel time through water, T_r the two way travel time through the reef. The velocity of the reef material can be calculated from the expression $(V_r)(T_r) = (V_w)(T_w)$ [Gregory and Kroenke, 1982].

thickest.   Beneath this is a series of flat-lying reflectors interpreted as lagoonal muds which are again thickest in the middle portion of the profile.   The velocities, travel-times and maximum thicknesses for these three layers are given in Table II.

TABLE II

PELAGIC CAP VELOCITIES, TRAVEL-TIMES, THICKNESSES

	Velocity (km/s)	Travel-time (s)	Maximum Thickness (m)
Pelagic cap	1.63	0.14	114
Oolitic limestone	3.83	–	35
Lagoonal mud	2.0	0.08	80

The velocities of the pelagic and oolitic layers are taken from Heezen et al., (1973). The oolitic particle velocity was determined to be 3.83 km/sec [Heezen and MacGregor, 1973] which is in good agreement with that determined by others [Press, 1966; Furumoto et al., 1970].

The interpretations of these layers and their thicknesses (Table II) agree very well with Jones (1973) who used sonobuoy data to compute a velocity of 1.6 km/sec for the pelagic cap and 3.85 km/sec for the oolitic limestone. Below the lagoonal mud is the irregular top of two other components, the reef complex and the volcanic basement. The reef is not continuous across the profile but is indicated only on the flanks where the reef community grew around the edges of the lagoon (see Fig. 8). The maximum thickness of the reef is 0.1 second of reflection time. The velocity as calculated by the method of Gregory and Kroenke (1982) ranges from 3.0-4.1 km/sec, giving a thickness of 150-205 m. The irregularity of the volcanic basement is probably due to erosion before the seamount became an atoll. Subsidence apparently was fast enough that the seamount was not completely leveled, but not fast enough to prevent reefs and a lagoon from forming for a short time.

The foregoing interpretation of the seismic reflection records are based on copies of the DSDP Leg 89 analog shipboard seismic refraction records [R. Moberly, pers. comm., 1985]. Whitman (1985) has independently interpreted the digitally collected seismic data of the Leg. The essential points of my interpretation agree with hers.

The post-eruptive depositional history of Ita Mai Tai is well recorded in the drilling record from Site 202 (Fig. 2). A 75 m thick

Globigerina sand and sandstone of middle Eocene and early Pliocene age overlies 35 m of lagoonal oolitic limestone of indeterminate age. Below this is a layer of lagoonal coraliferous mud at least 45 m thick containing a few fragments of basalt and feldspar indicating that the volcanic basement is close to outcropping in this area [Heezen et al., 1973; Hesse, 1973].

Neither the reef complex nor the basement were directly sampled in any of the DSDP holes. However, a number of dredges taken by the R/V Kana Keoki in 1981 did sample the reef outcrop, the lagoonal deposits, as well as slump or terrace deposits. A schematic cross-section of a flank of Ita Mai Tai reveals all of the components that comprise the top of the seamount (Fig. 7). Nemoto et al. (in prep., 1985) have classified the pelagic, oolitic, and lagoonal layers as the upper transparent layer (Fig. 7).

If all of the sediment layers and reef complex are stripped away, a map of the depth to basement remains (Fig. 8, K. Nemoto, in preparation). Along profile A-A' (Fig. 3) the basement rises to a central peak. In fact, the summit area has two high areas of basement, and a third down the southwest spur. The basement map shows the areal extent of the erosional remnants of the original volcano. It is not difficult to imagine looking at an aerial photo of a present day analog, Tahiti for example, and seeing the volcanic remnants standing above the lagoon and fringing barrier reef. If these are erosional remnants then Ita Mai Tai must have subsided a total of 2090 m which is comparable to other seamounts in the area such as Kwajalein (2000 m) and Enewetak (1900 m) [Jones, 1973].
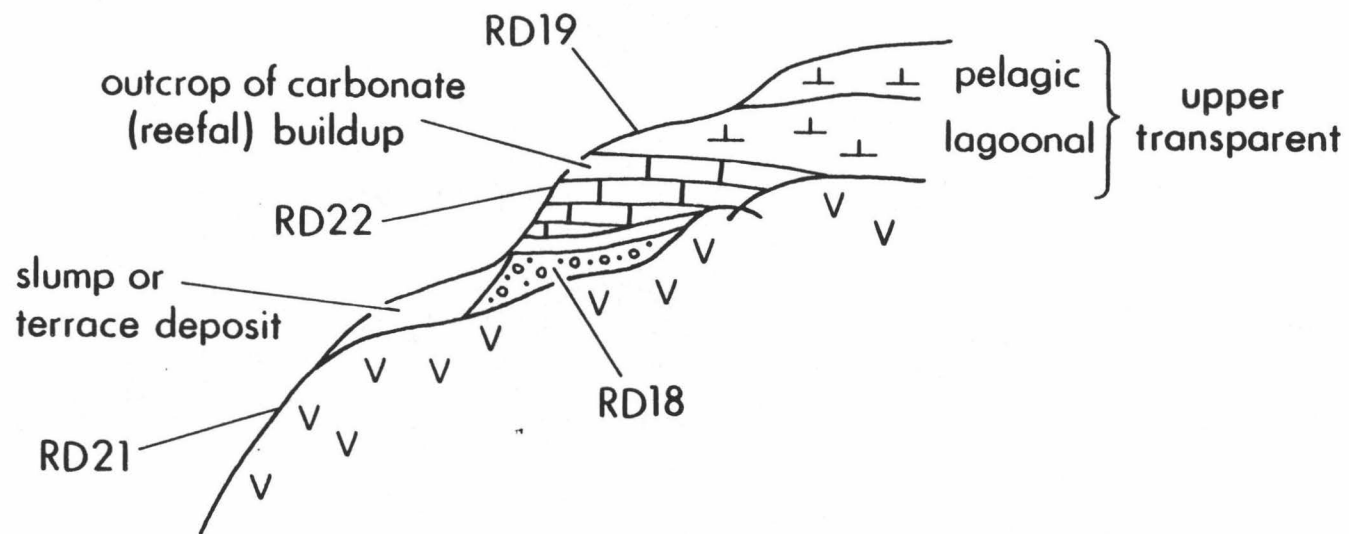
Figure 7. Cartoon showing the components of the pelagic cap
[Nemoto, et al., in press, 1985]. Also indicated
are the locations of the dredges from KK810626
Leg 2.
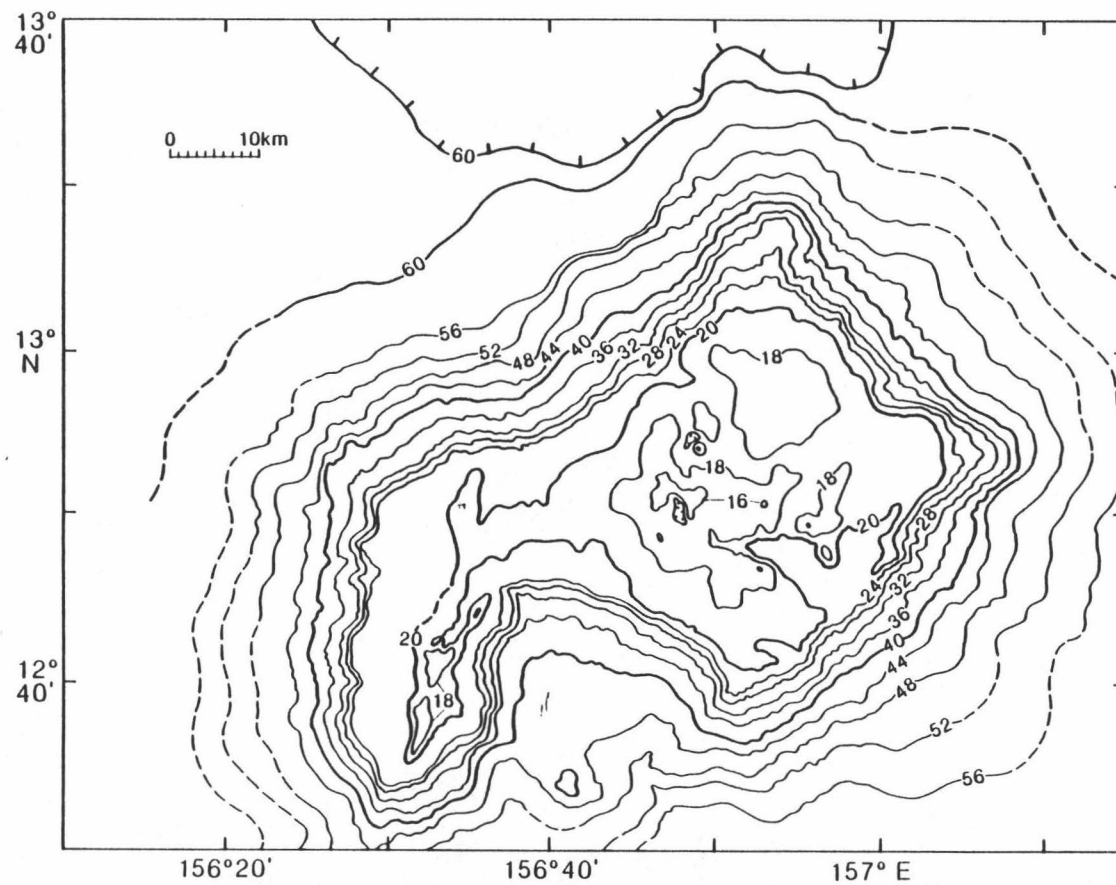
Figure 8. Map of Ita Mai Tai showing the depth to basement
in meters X 100. The sediment thicknesses down
to volcanic basement have been removed.

GRAVITY

Density determinations on the edifice itself are not available. Dry density measurements of basaltic lavas from Oahu made by the Hawaii Institute of Geophysics ranged from 2.3 to 2.9 g/cm^3 [Strange et al., 1965]. Investigations off the island of Hawaii reveal that the size of vesicles in the lavas decrease with water depth. Values for surface lavas average 2.2 g/cm^2 and 2.9 g/cm^2 for lavas at a depth of 1 km [Strange et al., 1965]. The densities assumed in this study are : water 1.03 g/cm^3, sediments 1.9–2.1, volcanic edifice 2.3–2.9, oceanic crust 2.9, and oceanic mantle 3.4.

The configuration of the free-air gravity anomaly over the seamount is shown in Figure 9. Generally, the shape of the anomaly follows the bathymetry. The amplitude ranges from a maximum value of 254 mgal over the summit to a low of –69 mgal observed over the moat on the southeast side of the edifice. The total amplitude range of 323 mgal for Ita Mai Tai is exceeded in the north Pacific only by the much larger and shallower Hawaiian-Emperor chain. The shape of the anomaly also suggests that there was probably only one main volcanic conduit.

MODEL STUDIES

In order to find the best fitting model for Ita Mai Tai the observed gravity data were estimated for 980 grid points at about 5 km intervals. Ten polygonal layers with vertical sides were used to model the bathymetry (Figures 10 and 11). The observed gravity was
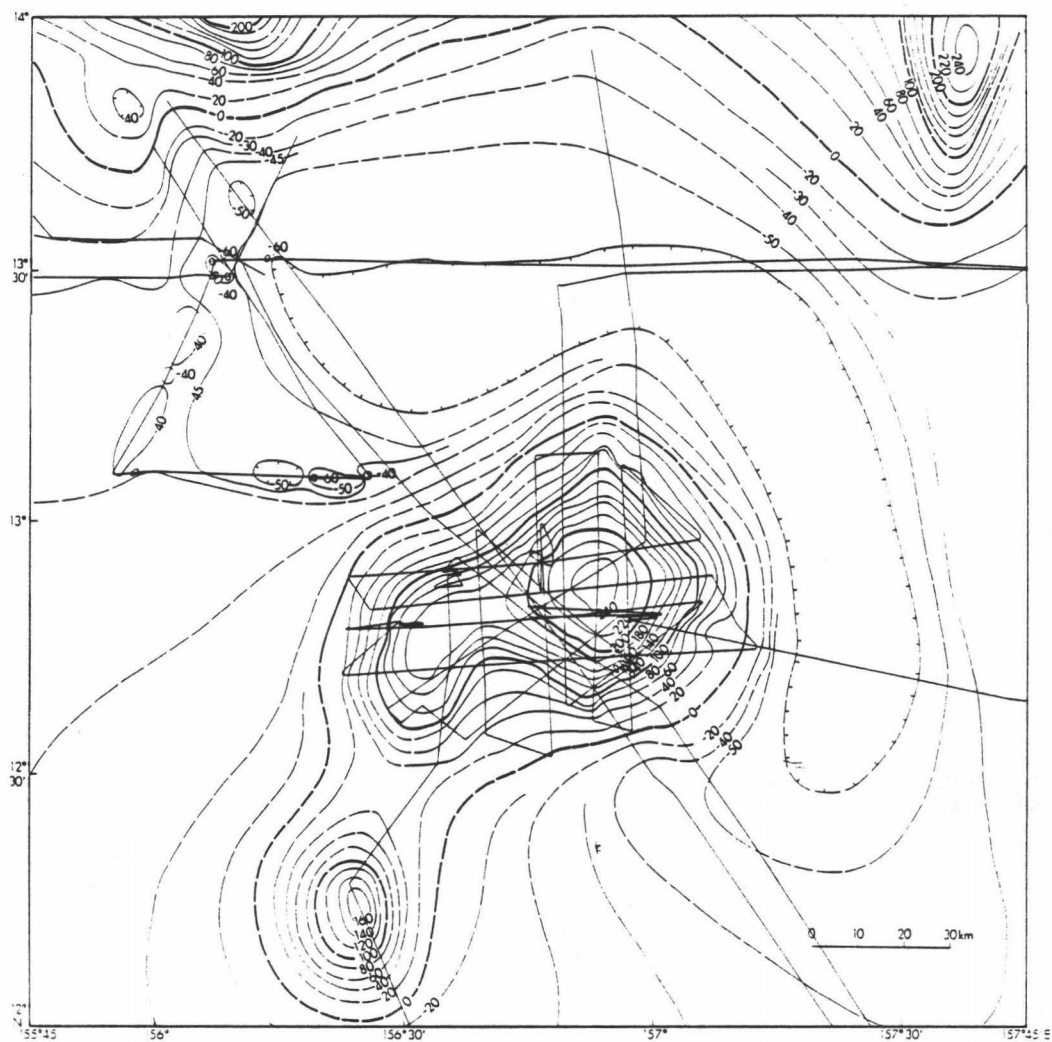
Figure 9. Free-air anomaly map in mgals of Ita Mai Tai
Guyot and surrounding sea floor. Ship tracks are
indicated by black lines.

a

b
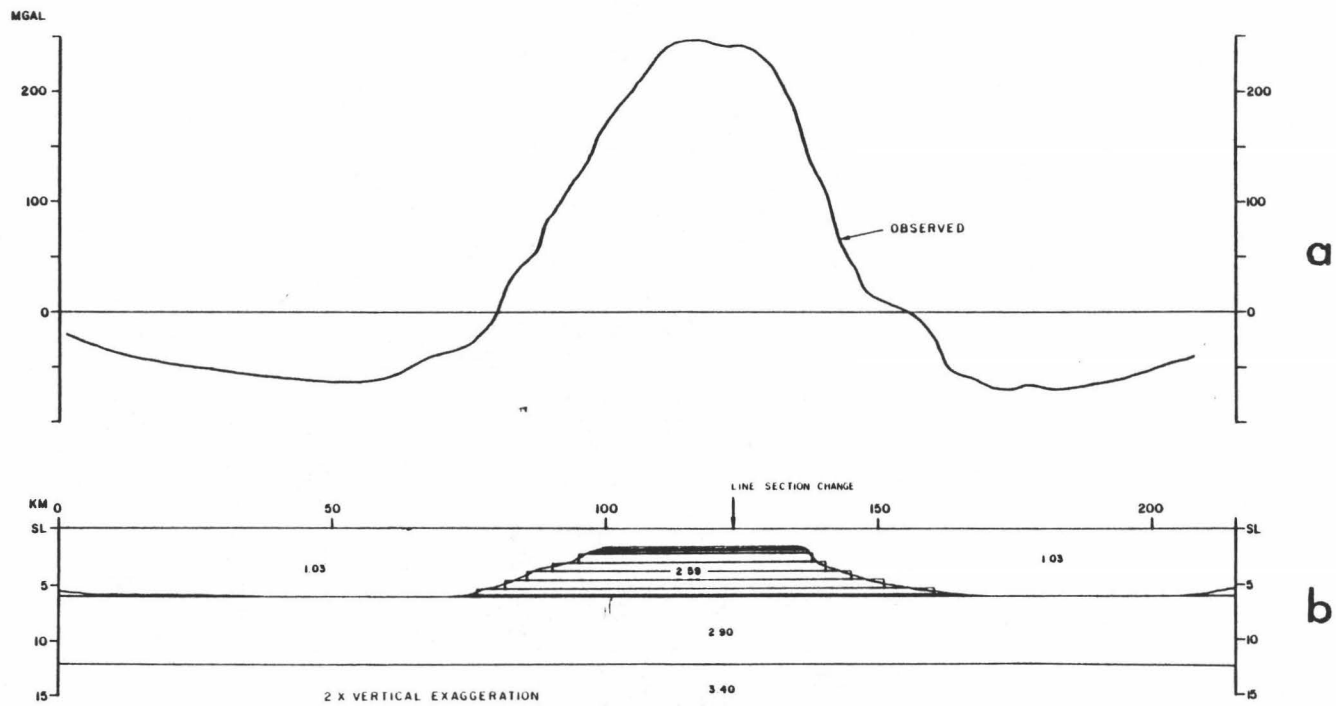
Figure 10. (a) The observed gravity anomaly over Ita Mai Tai
showing the moats on both sides. (b) Bathymetric
model A showing the ten prisms and densities
used.

24

Figure 11. Plan view of the bathymetric prisms for model A. The two straight lines show the position of the transect used in the model studies.

then inverted using a modified Talwani and Ewing 3-D approach [Plouff, 1976]. This technique uses a linear least squares analog to determine the average density of the seamount and assumes internal homogeneity from summit to sea floor. The 3-D method was used because the 2-D approach over-corrects the gravity field by 18 percent over the apex of a conical seamount with a 10° slope [Rose and Bowman, 1974].

The calculated density was 2.59 g/cm^3. Both the calculated anomaly for this model and the residual field (observed minus calculated) are shown in Figure 12. The shape of the anomaly closely resembles the original bathymetry. The calculated mean density value agrees well with values for other seamounts such as 2.5 g/cm^3 for Chautauqua Seamount [Schimke and Bufe, 1968], 2.6 g/cm^3 for an unnamed Atlantic seamount [LePichon and Talwani, 1965], and 2.48 g/cm^3 for Nagata Seamount [Sager et al., 1982]. There were areas however, where the fit could be improved, particularly over the summit area and over the basin to the east of the seamount.

Once the overall density was calculated, geological and seismic reflection data were used to constrain the model. A dense volcanic conduit was added, extending from the top of the seamount to the oceanic crust. The density used for the conduit was 2.95 g/cm^3, in accordance with the measured densities of 2.8 g/cm^3 for eclogite from Koolau Caldera and 3.0 g/cm^3 for nephelinite from Salt Lake Crater on Oahu [M. Manghnani, pers. comm., 1985]. The average bulk density of the model then changes to 2.70 g/cm^3.

Prisms representing the sediment filled basins and incorporating the seismic reflection data were added to the model. The drilling
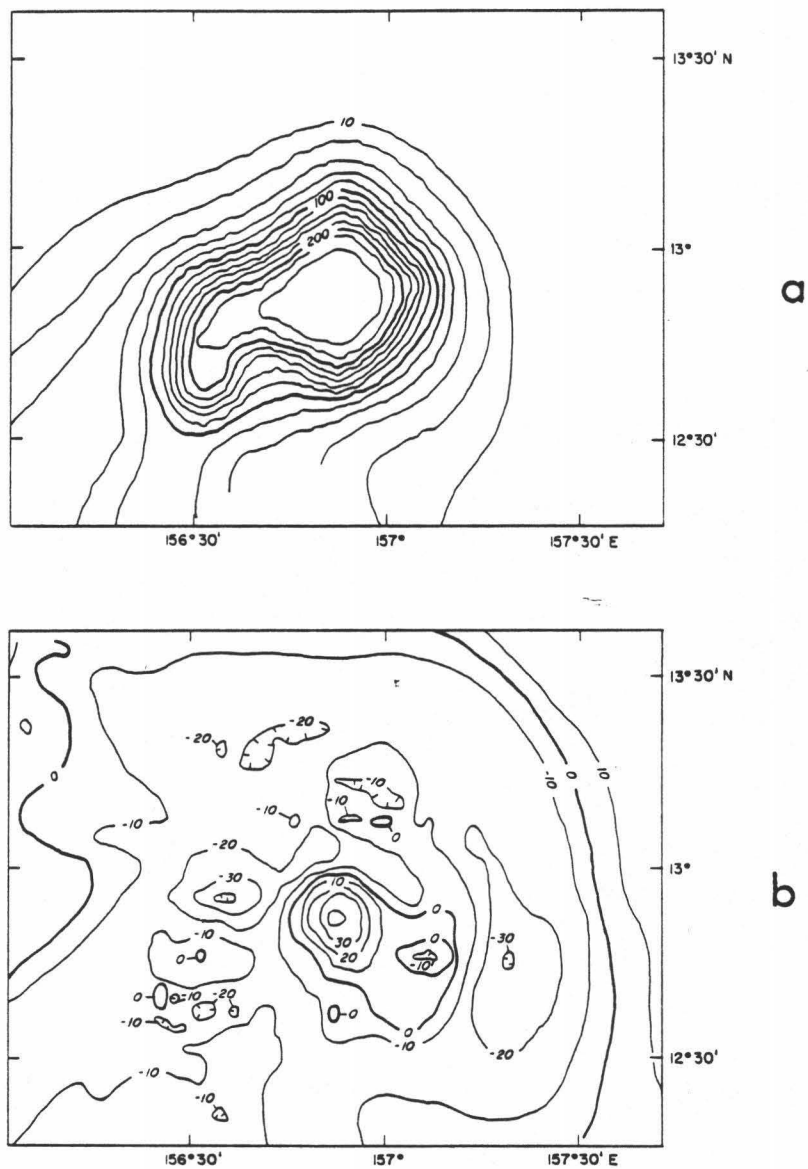
Figure 12. (a) Calculated gravity field in mgals for model
A. (b) the residual field (observed minus
calculated).

record of Site 585 provided velocities which were converted into densities after G. P. Woollard (1962). A small amount of crustal thickening was added to the model directly below the seamount (Fig. 13).

Two slightly different approaches were used to achieve the final models. Model B assumes identical sediment bodies to the north and east (Fig. 13), although the eastern basin was not directly sampled, and 1.0 km of crustal thickening beneath the seamount (body 12, Fig. 14). The calculated and residual anomalies are shown in Figure 15. The maximum difference between the observed and calculated along the northern track is about 25 mgal. A profile of the observed and the calculated gravity anomalies is shown in Figure 16. The goodness of fit parameter is 4.87 [Richards et al., 1967], showing that the model adequately describes the observed anomaly.

Model C is very similar to model B except that there is one less sediment body in the southeast basin, indicating a shallower depth to acoustic basement, and crustal thickening of 1.5 km which extends easterly to the edge of the model (Fig. 17). The plan view of the prisms is shown in Figure 18. Figure 19 shows the calculated and residual anomalies. The greatest difference from model B is a smaller low that has been repositioned farther south. Again, the maximum residual is about 25 mgal, along the northern track. When a profile of the observed field is superimposed on the calculated gravity the good fit is readily seen (Fig. 21). The goodness of fit is 4.96, slightly better than model B.
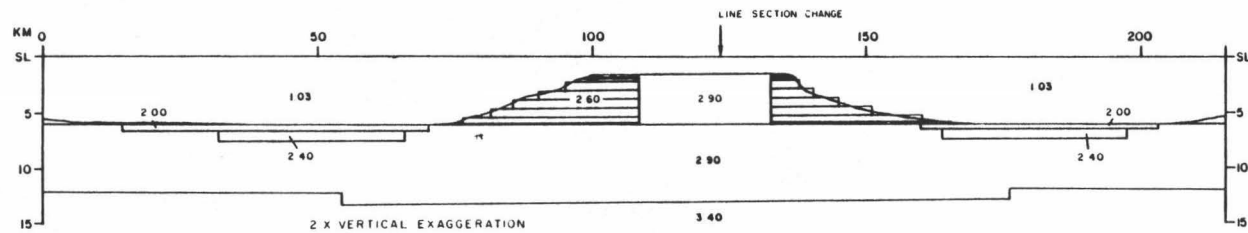
Figure 13. Cross-section showing the bathymetric prisms used
in model B. Volcanic conduit, sediment bodies,
and crustal thickening added.
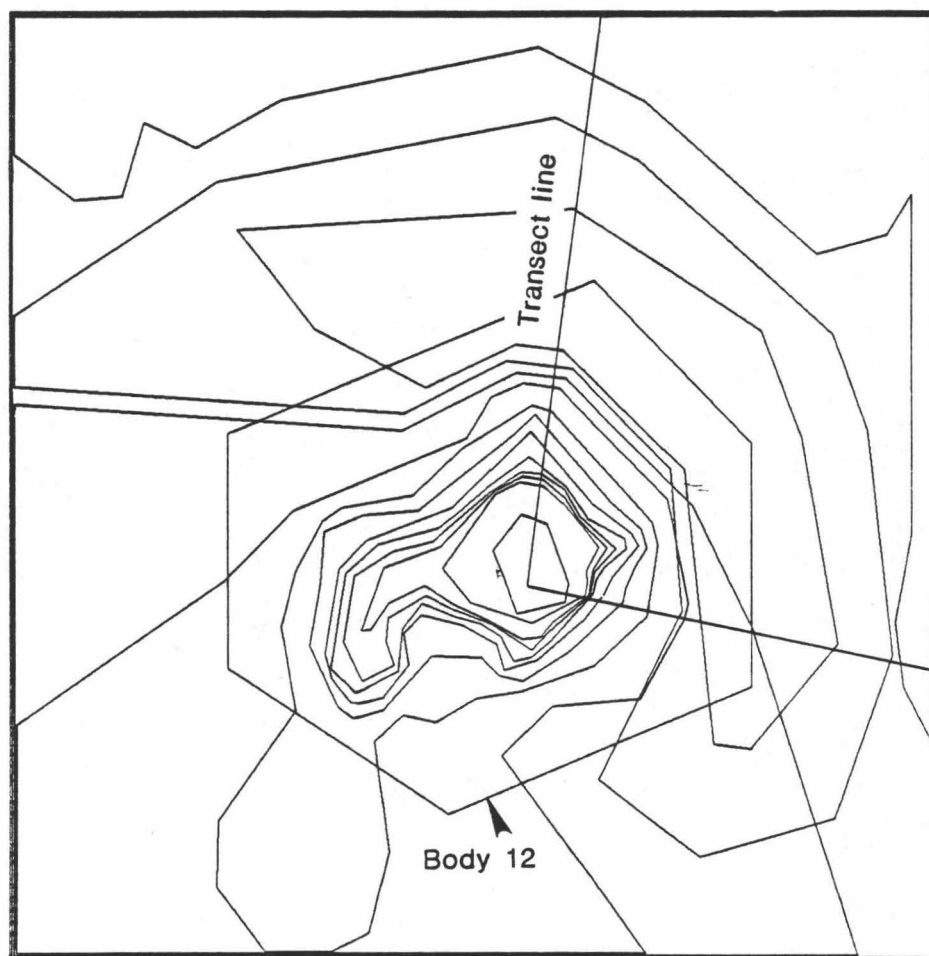
Figure 14. Plan view of the bathymetric prisms for model B.
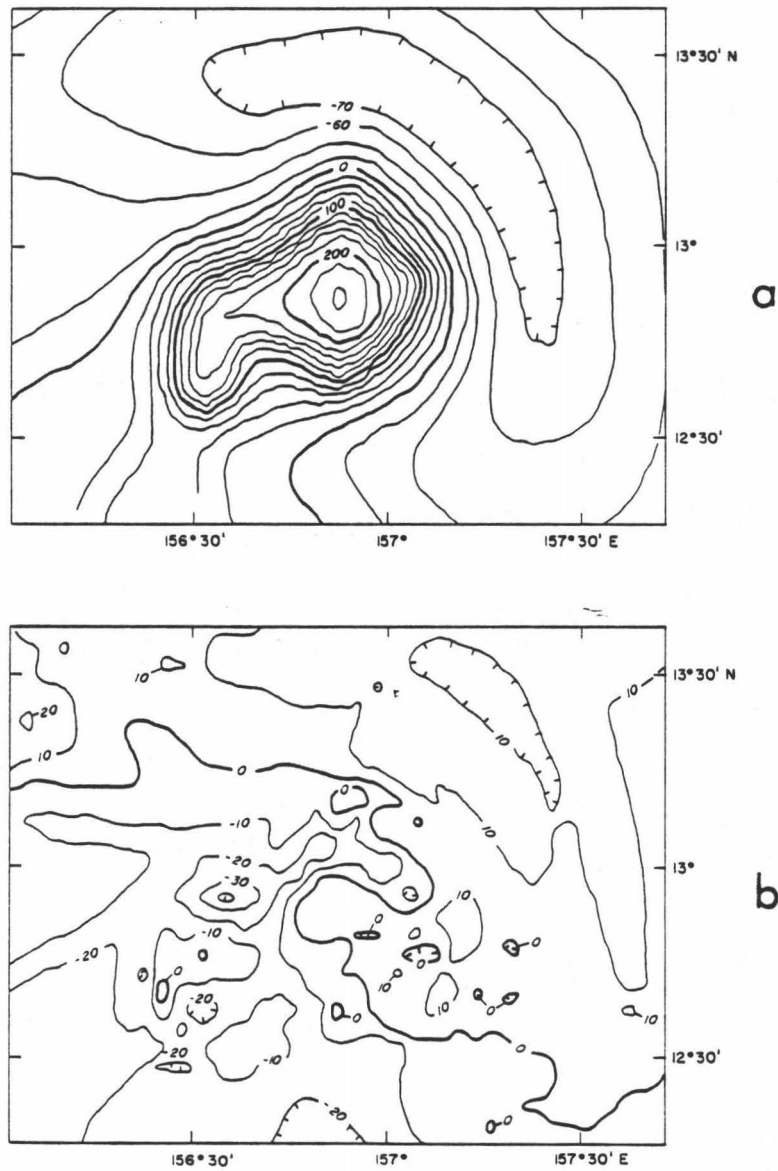
Figure 15. (a) The calculated gravity field in mgals for
model B. (b) The residual field.
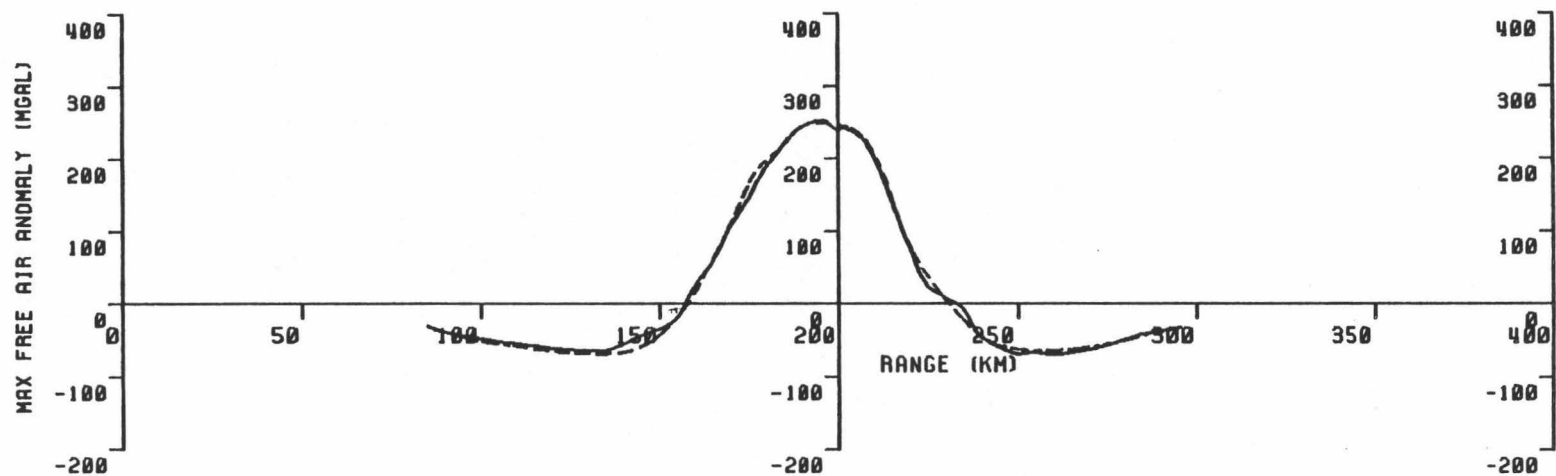
Figure 16. Cross-section along track of the observed gravity
anomaly (solid line) and model B (dotted line).
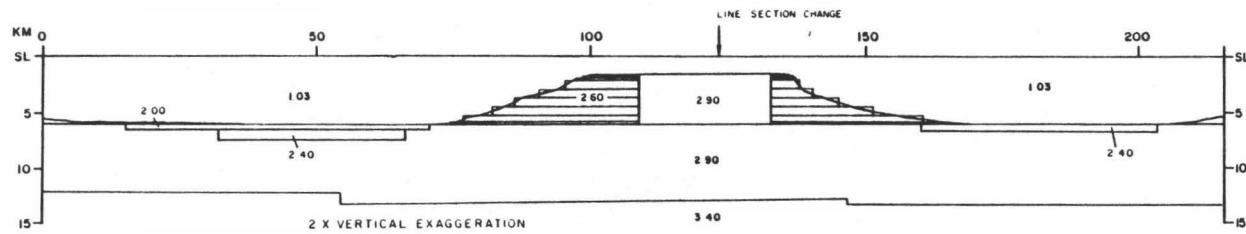
Figure 17. Cross-section showing the bathymetric prisms used in model C.

Figure 18. Plan view of the bathymetric prisms for model C.
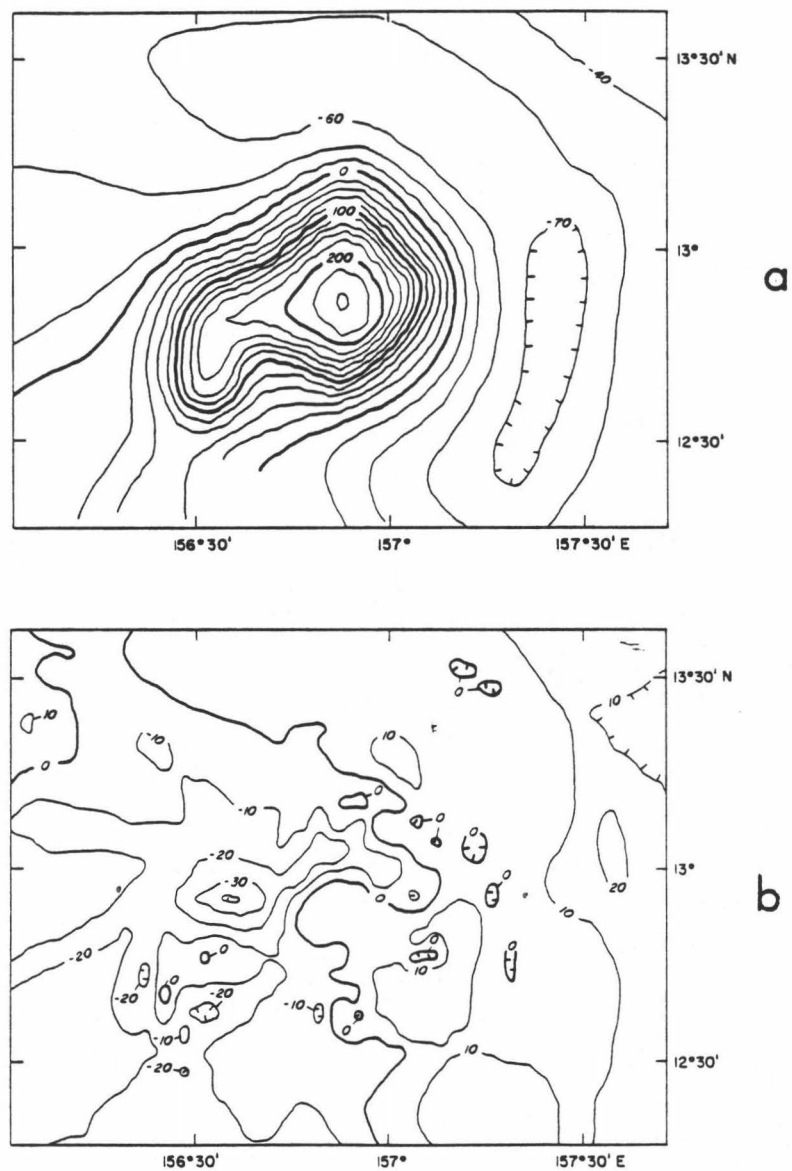
Figure 19. (a) The calculated gravity field in mgals for
model C. (b) The residual field.
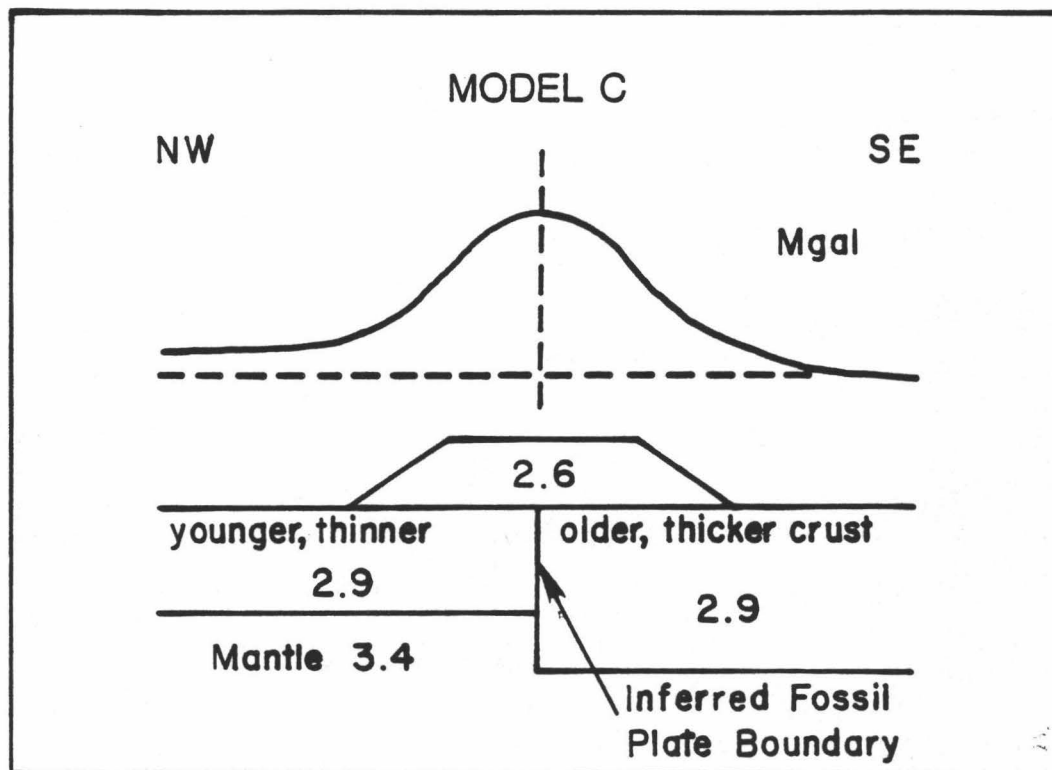
Figure 20. Cartoon showing the two different thicknesses of oceanic crust on either side of Ita Mai Tai perhaps showing a fossil plate boundary.
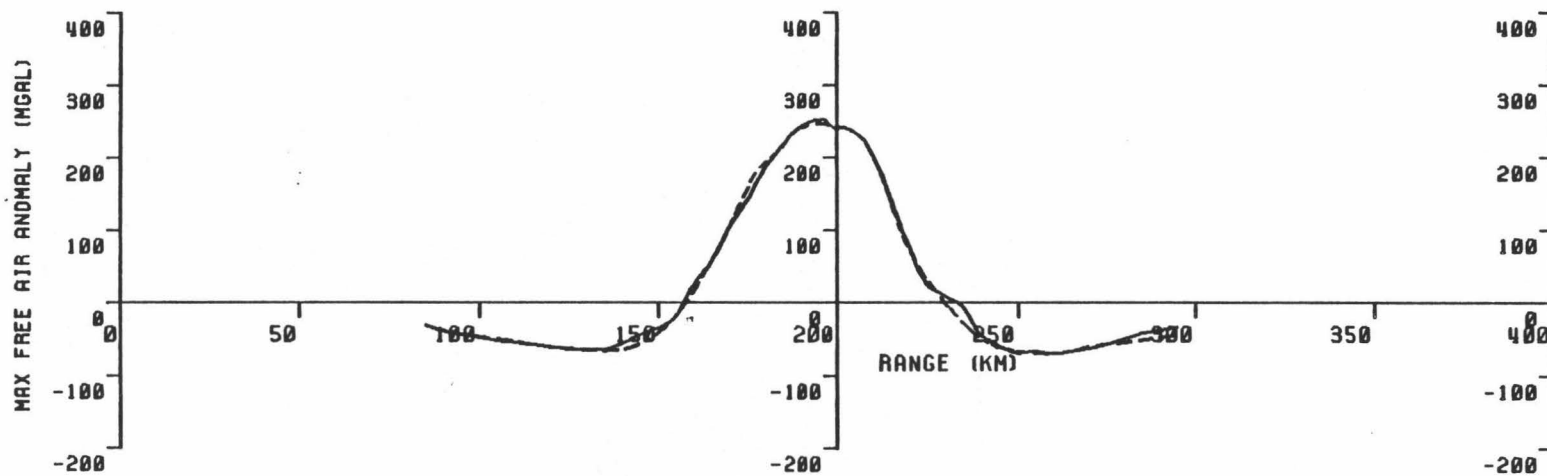
Figure 21. Cross-section along track of the observed gravity
anomaly (solid line) and model C (dotted line).

The difference between the two models' calculated anomalies is negligible (Fig. 21). Both adequately explain the observed data. The seismic data however would seem to give more credibility to model C with its shallower southeast basin because it does not require the assumption that opaque layers (lava flows, sills, etc.) mask deeper basement, but this model does require the assumption of changes in crustal thickness.

Thus, Ita Mai Tai appears to be almost completely locally uncompensated. This rather dense seamount is, in effect, perched on oceanic crust 6-7.5 km thick causing at most only 1.5 km of crustal downwarping. A two-ship multichannel seismic experiment carried out by Lamont and the Hawaii Institute of Geophysics [Watts et al., 1985] found that only 3 km of the 8 km of crustal thickening under Oahu could be explained by lithosphere flexure under a superimposed load. This seismic interpretation is questioned by D. Lindwall [pers. comm., 1985], however, whose synthetic seismic models may be completely explained by flexure. Most of the remaining thickening may be caused by sill injection or magma chambers in the crust. The lack of isostatic compensation in Ita Mai Tai may be the result of midplate eruption on thick inelastic lithosphere with little or no sill injection into the crust.

COMPARISONS WITH OTHER WESTERN PACIFIC SEAMOUNTS AND ISLANDS

The gravity field of Ita Mai Tai was compared with 58 seamounts and 38 islands and atolls in the North and South Pacific Oceans and a

few in the Atlantic (Appendix C). Only those seamounts that were well-surveyed and had both bathymetric and gravimetric data were used in the study. The maximum free-air anomaly is plotted against the minimum depth to the top of the seamount in Figure 22. Bouguer anomalies are plotted for islands. The resulting gravity-depth relation mean is $z = -16g_z + 3800m$ where z is the minimum depth to the top of the seamount and g_z is the maximum free-air gravity anomaly in mgal observed at the sea surface. As might be expected, there is a general inverse relationship between depth and gravity anomalies. This relation varies for different seamount groups. For seamounts of the same size and depth the observed gravity anomaly can vary as much as 200 mgal. Also, there are relatively few seamounts in the depth range from 0 to 1 km. This may be a sampling bias since there may be as many as 55,000 seamounts in the Pacific [Batiza, 1982] and our study population is relatively small.

Ita Mai Tai (an uncompensated seamount) and Sio Guyot (a fully compensated seamount in the Mid-Pacific Mountains [Kellogg and Ojugiofor, 1985]) are end members in terms of their local isostatic compensation. Ita Mai Tai has a maximum free-air anomaly 120 mgal higher than Sio, even though Ita Mai Tai is much smaller and deeper. Figure 23 is a fishnet 3-D representation of the sea surface gravity fields of Sio and Ita Mai Tai.

The same gravity-depth relation was plotted for separate seamount groups such as the Musicians, Marshalls, and Emperors (Fig. 24). A least squares line was fit to five seamounts in the eastern Marshalls around Majuro, the group closest to Ita Mai Tai. The line is almost
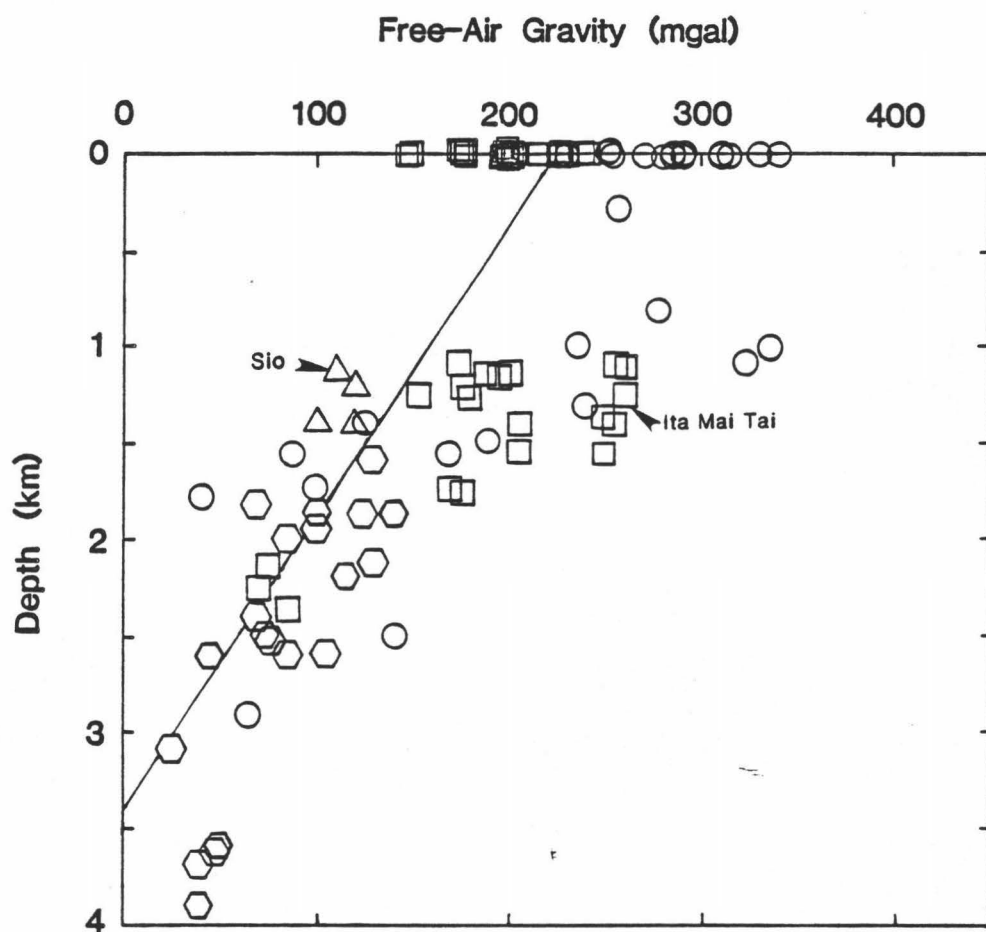
Figure 22. Maximum free-air gravity anomalies and minimum
depth for seamounts and islands of the Western
Pacific (Kellogg and Wedgeworth). The Mid-
Pacific Mountains are shown as triangles; the
Marshall Islands and seamounts are shown as
squares.
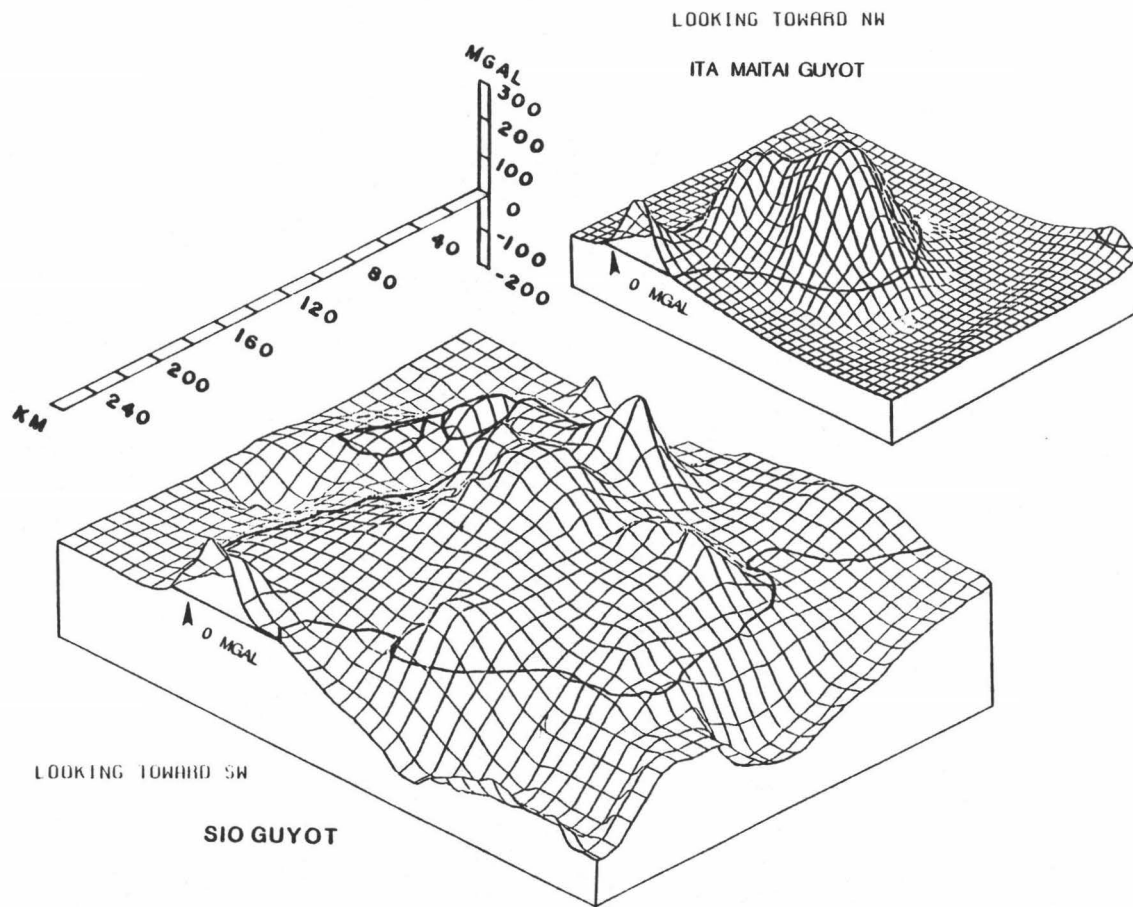
Figure 23. Three-dimensional fishnet representations of the free-air gravity anomaly fields over Sio and Ita Mai Tai Guyots from Kellogg, et al. (1984).

MAX FAA (MGAL)
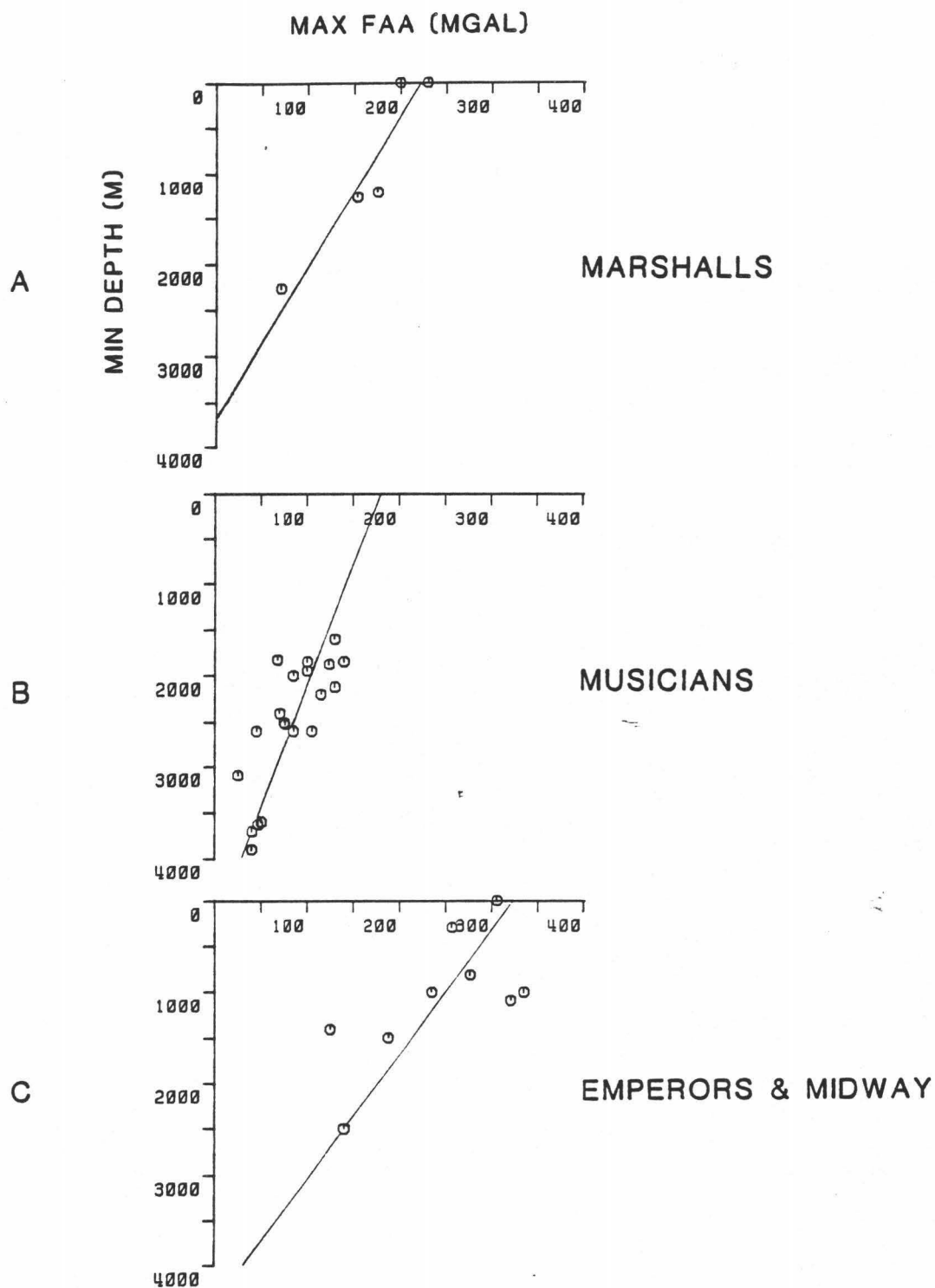
Figure 24. Plots of the maximum free-air anomaly vs. minimum
depth of three different groups of seamounts.
Best fitting least squares lines are shown.

parallel to the trend for the Musicians. The large scatter in Figure 24 probably represents a difference in local isostatic compensation and thickness of the crust beneath the seamounts.

The gravity values of the line $g_z = (3800m - z) / 16.0$ in Figure 22 were subtracted from the gravity values for the observed seamounts (Appendix D) and the residual values were plotted on a map (Fig. 25) to see if there was a spatial systematic variation in the seamount gravity-depth relationship. There is a distinct break between the eastern and western Marshalls. The positive residuals, over 100 mgal, may indicate mid-plate eruptions away from ridge crests. The negative residuals, as low as -78 mgal, in the middle of the Marshall Island group and in the Mid-Pacific Mtns., suggest possible ridge crest eruptions for large areas of this map. It appears that isostatic compensation may follow regional patterns.

Various levels of Airy-Heiskanen local isostatic compensation were used to explain the differences in observed seamount gravity fields. The shape of the seamounts was assumed to be simple right cones and frustrums of cones. Jordan et al. (1983) has suggested that two important parameters in characterizing seamounts are the height to basal radius ratio (h/r) and the flatness ratio (r_2/r_1) where r_2 is the radius of the base and r_1 is the radius of the summit (Appendix E). The resulting ratios were plotted for 62 well surveyed Western Pacific seamounts in Figure 26. Five morphologic seamount models were constructed using the mean h/r and r_2/r_1 ratios: two small conical shaped seamounts, two guyots and one atoll (Fig. 26). Each was then modeled assuming 0 and 100 percent local compensation.
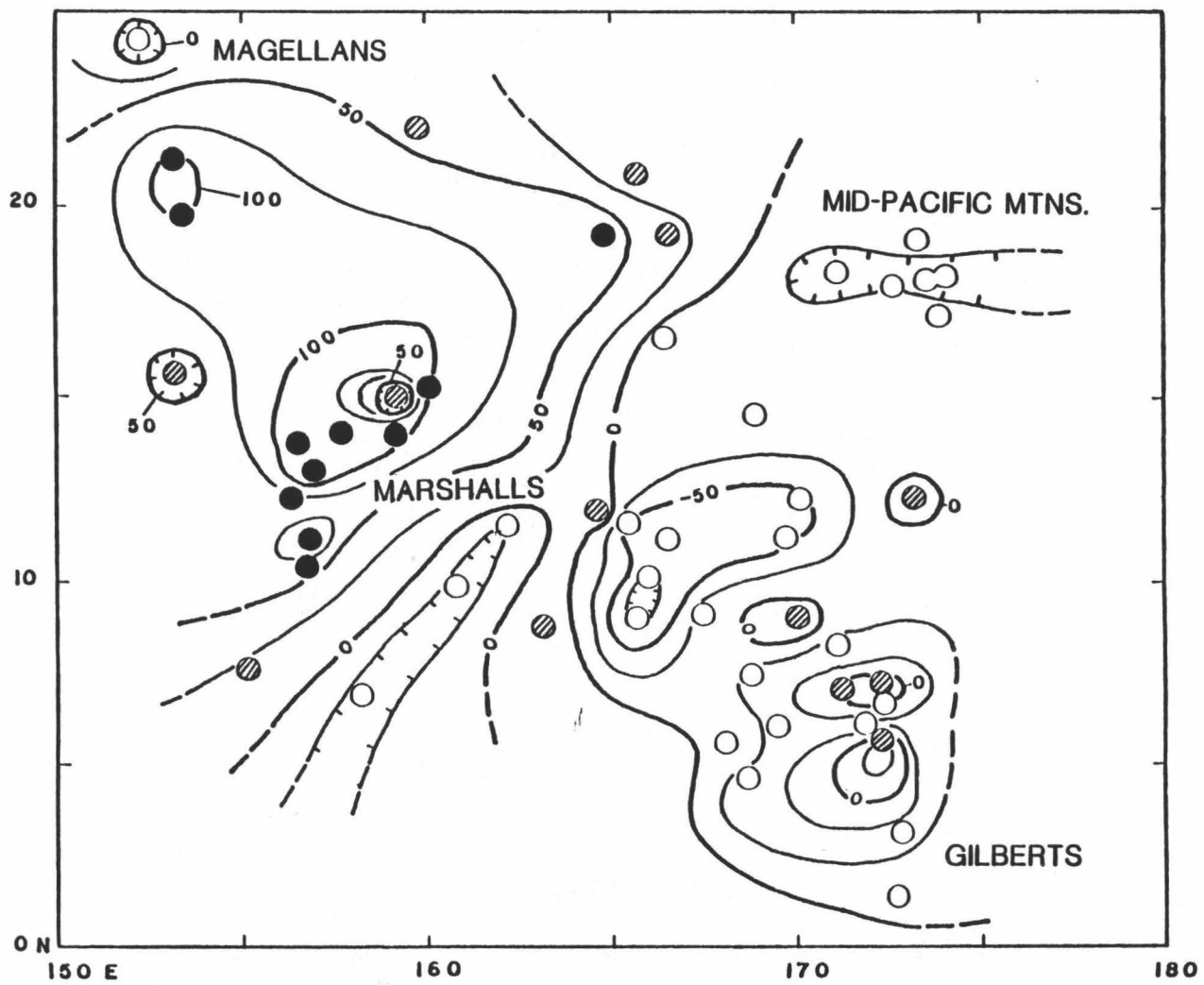
Figure 25. Regional isostatic compensation map. Values in mgals.
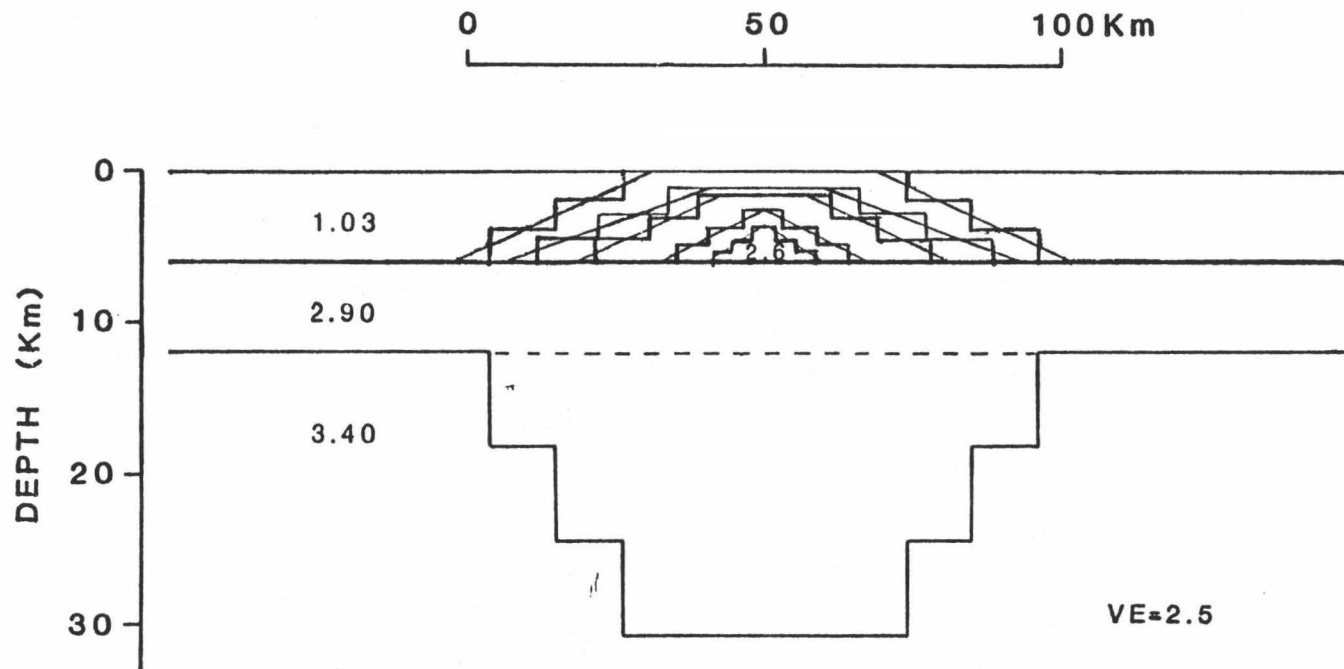
Figure 26. Five theoretical seamount models. Root shows 100 percent local compensation at depth. Dashed line represents no root, or 0 percent local compensation.

The calculated gravity fields for the five uncompensated and five compensated models are shown in Figure 27. When the two sets of models are compared (Fig. 28) several things become apparent. The compensated models have moats, the uncompensated do not. There is less contrast between the models as the depth increases. There is as much as 200 mgal of difference in the models at the sea surface. When the two model sets are plotted versus depth (Fig. 29) each falls within a broad linear band. For seamounts below about 3.5 km the differences in the gravity effects of the compensated and uncompensated models are negligible at the sea surface. In Figure 30 the calculated gravity effects of the models have been superimposed on the plot of free-air gravity versus minimum depth (Fig. 22). A majority of the seamounts lie in the field between the lines of 0 and 100 percent compensation. Twenty-two (38%) are more than 100 percent compensated. Some of these over-compensated seamounts, such as Sio Guyot, are built up on plateau structures, increasing the thickness of the oceanic crust and root compared to the relief of the seamount. Ita Mai Tai and other nearby seamounts in the western Marshall Island group lie close to the 0 percent compensated line. The only seamounts that appear to be even less compensated than Ita Mai Tai are two of the Emperors, Suiko and Nintoku.

We also investigated whether or not the degree of compensation of a seamount could be used to predict the seamount's age relative to the underlying sea floor. The sea floor age at the time of eruption was plotted against the maximum free-air anomaly minus the theoretical 100 percent compensated line for six reliably dated seamount and island
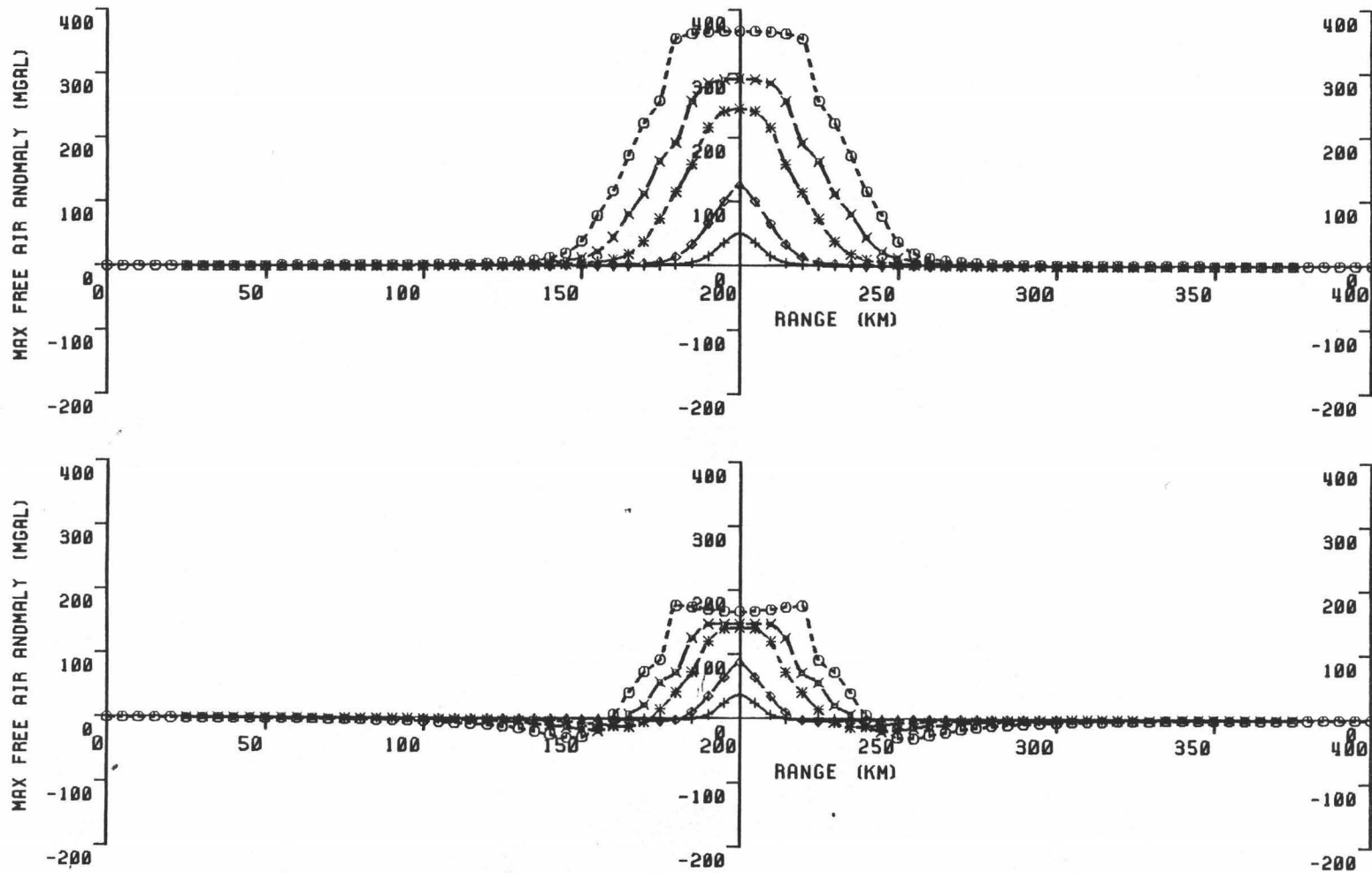
Figure 27. (a) Cross-sections of the calculated gravity
field produced by the five uncompensated seamount
models. (b) Calculated gravity field from the
five compensated seamount models.

47
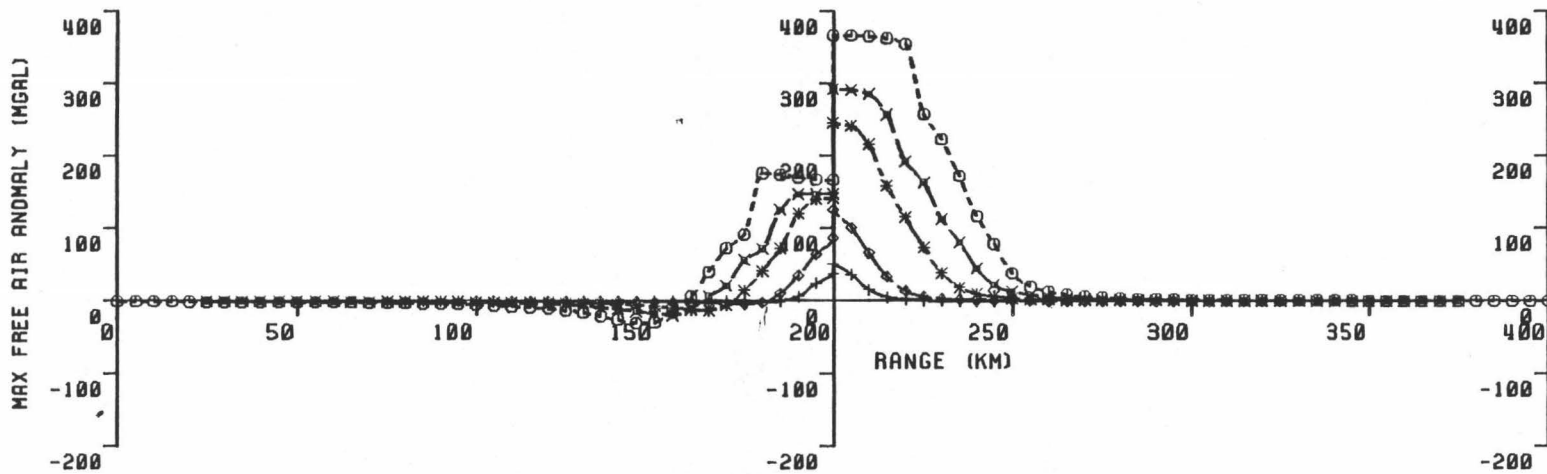
Figure 28. The 0 and 100% compensated gravity fields juxtaposed for comparison.
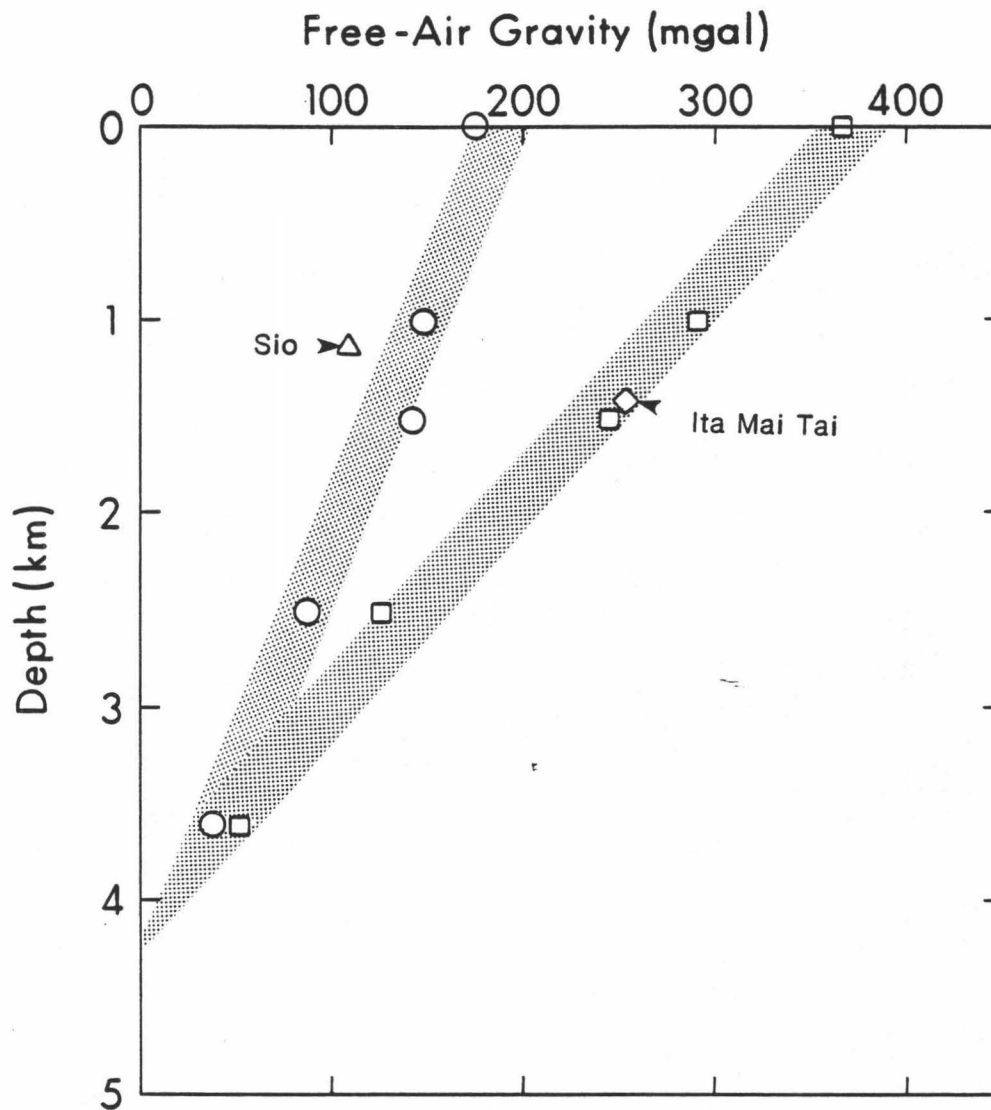
Figure 29. The ten models are shown on the gravity-depth
plot. Circles are 100 percent compensated,
squares 0 percent. The triangle is Sio Guyot and
the diamond is Ita Mai Tai.
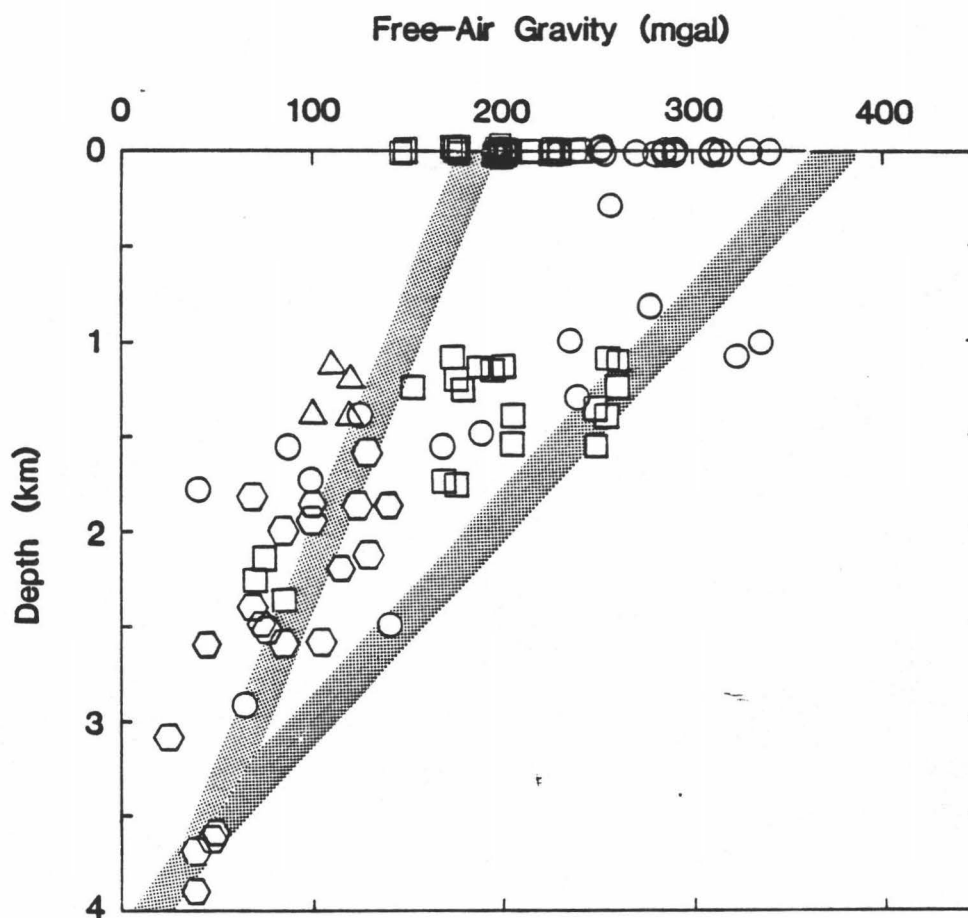
Figure 30. The 96 seamounts and their relationship to the fields of compensation. Squares = Marshalls, triangles = Mid-Pacific Mtns., hexagon = Musicians, circles = Hawaiian-Emperors, misc.

groups (Fig. 31) (Appendix F). There is good correlation, indicating that the older the crust is before a seamount forms on it the higher will be the resulting free-air anomaly. Knowing the gravity anomaly and the age of either the volcano or the sea floor, and given more data, perhaps this plot can be used as a predictive tool. Figure 32 is a map of the Pacific showing the locations of all the seamounts used in this study. We believe that all of the compensated seamounts were formed on sea floor less than 30 or 40 m.y. old. These seamounts may have been erupted near Cretaceous ridge crests rather than in a mid-plate event as has been previously hypothesized by others. The data values for all of the aforementioned seamounts are listed in Appendix H.
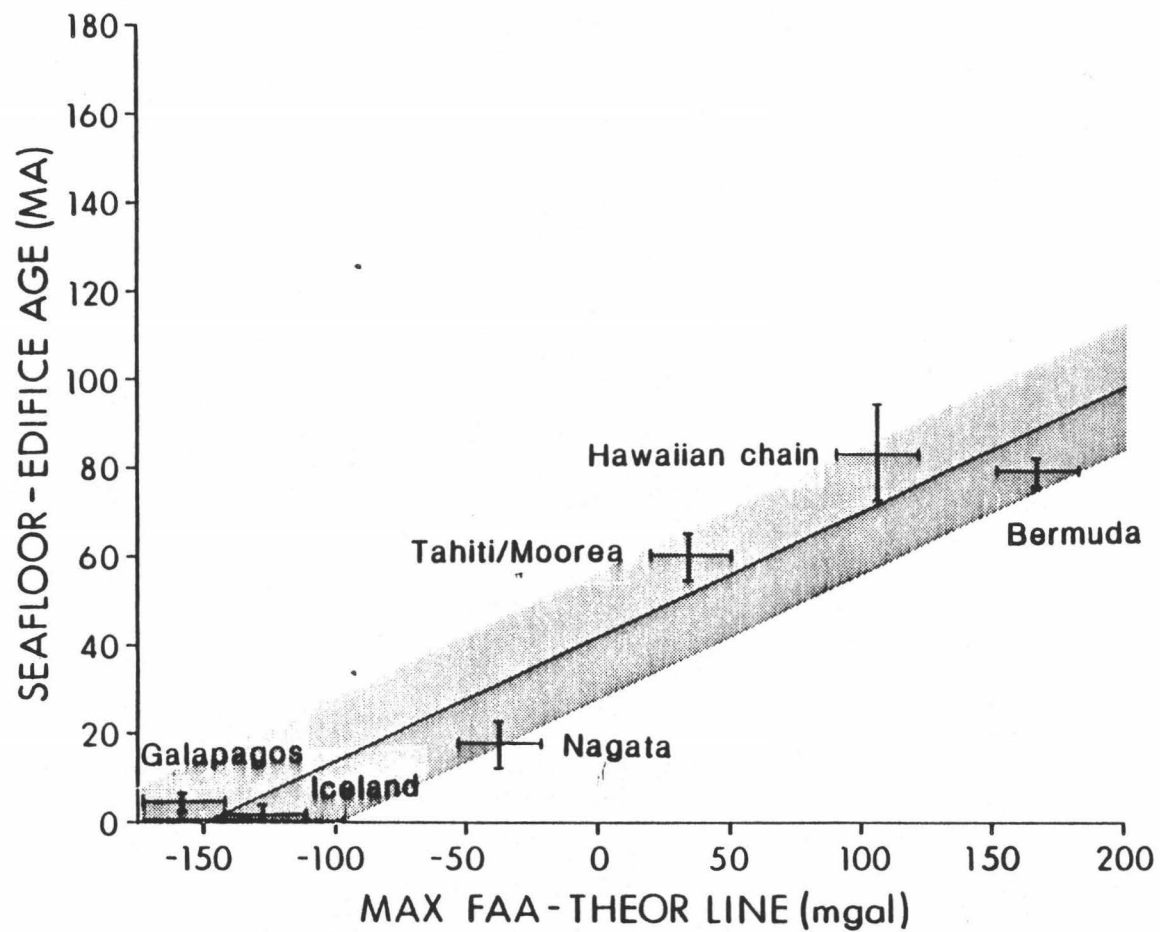
Figure 31. Plot of the age of the sea floor when formation of seamount occurred vs. the maximum free-air anomaly minus the line of 100 percent local compensation. Bars indicate range of error.
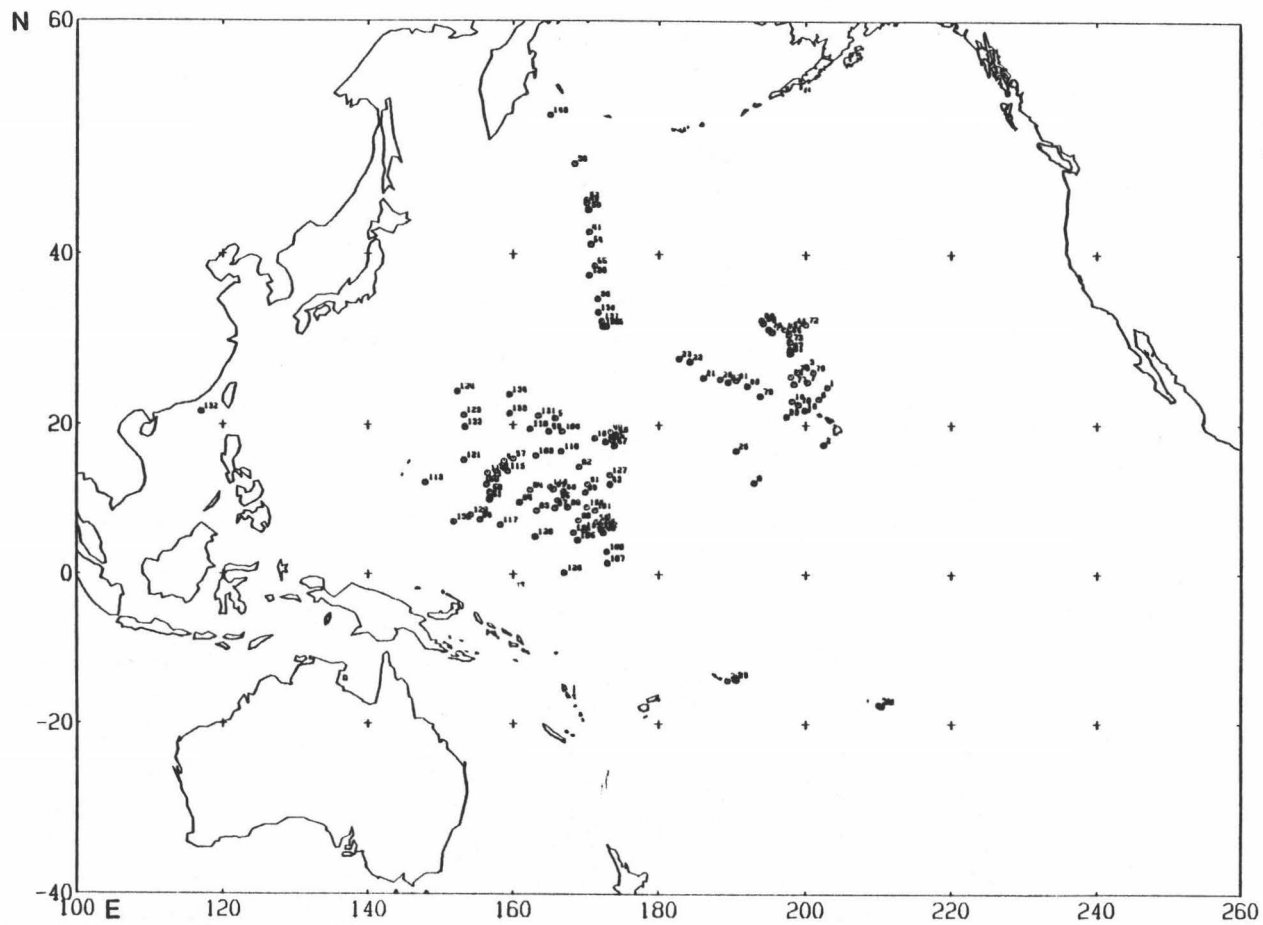
Figure 32. Map of the North Pacific Ocean showing the locations and catalog numbers of all seamounts studied. Ita Mai Tai is number 11, Sio is number 10.

CONCLUSIONS

1. Computer models show that Ita Mai Tai is a large uncompensated seamount that only requires an addition of 1.5 km of crustal thickening.

2. The lack of compensation resulted from eruption on thick inelastic oceanic crust at least 30-40 m.y. old.

3. Ita Mai Tai first erupted during the Aptian/Albian and possibly again during the Eocene. The volcanism is recorded in volcaniclastic deposits in the basins north and southeast of Ita Mai Tai.

4. Seismic reflection records may indicate the existence of an unrecognized fossil plate boundary which would obviate the need for a magma source body working its way through such thick crust.

5. There is an inverse relationship for free-air gravity versus minimum depth for 96 seamounts and islands in the Pacific. For seamounts at a given depth the observed gravity anomaly can vary as much as 200 mgal which represents a potentially large source of error in bathymetric prediction using satellite altimetry data. However, seamounts with similar degrees of compensation form clusters and accurate prediction may be possible within those clusters.

6. After normalizing gravity values for seamount depth by subtraction from a line for a representative seamount cluster, the resulting map reveals a distinction between the uncompensated seamounts in the west (mid-plate eruptions) and the compensated seamounts in the east (ridge crest eruptions).

7. A majority of the surveyed seamounts lie in a field between the lines of 0 and 100 percent compensation for seamount models of different sizes at different depths.

8. Because as oceanic lithosphere grows older it thickens and cools and is less likely to bend under the load of a seamount, there is less chance that an erupting seamount will be locally compensated. Therefore, the older the crust at the time a seamount forms on it the higher will be the seamount's resulting gravity anomaly. The maximum gravity anomaly of a seamount may tell us something about the age of the sea floor where it formed, which would be especially useful in areas where there are no magnetic lineations.

APPENDIX A

<u>Ita Mai Tai Volume Calculations</u>

The volume of Ita Mai Tai Guyot was calculated using two different methods. First, the volume can be approximated by the frustrum of a right cone (Figure 33). The volume of a frustrum is given by

$$V = 1/3 \quad h \ (R^2 + Rr + r^2)$$

$$\text{where } R = 45 \text{ km}$$
$$r = 17.5 \text{ km}$$
$$h = 4.5 \text{ km}$$

The volume then is 14,696.8 km^3.

However, the bathymetry shows that Ita Mai Tai is not a perfect frustrum so a computer program was written in collaboration with John Williams that calculates that volume by slicing the bathymetry of Ita Mai Tai into eleven horizontal prisms. Each of these prisms simulates the bathymetry at a given depth. The Plouff gravity program in this paper used the same set of prism parameters to find the density of the seamount. An initial point must be entered into the program from which a line can be drawn to each of the vertices in the prism, forming triangles (Figure 34). The volume then is simply a function of the area of each triangle and the height of the prism. The

procedure is repeated for each prism. The resulting volume is 14,785 km^3, in very close agreement with the first method.

The volume of Ita Mai Tai is very much larger than the mean of 609 km^3 for North Pacific volcanoes [Batiza, 1982], probably because his mean reflects the greater abundance of smaller seamounts.
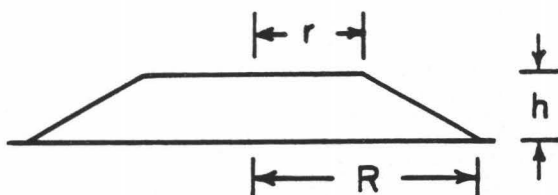
Figure 33.   Dimensions of a seamount frustrum.
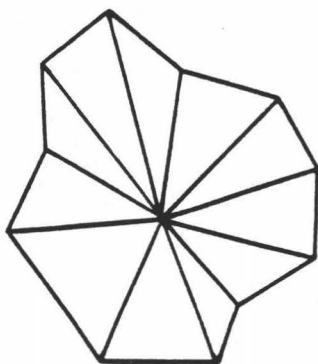
Figure 34.   Typical prism used in volume calculations.

APPENDIX B

Acoustic units were identified on HIG cruise KK810626 Leg 2 by similarity in acoustic character with those of the DSDP Leg 89 for the trackline across the northern basin. Average layer thicknesses were based on the HIG trackline in order to facilitate the gravity modeling. Unit boundaries were picked as follows:

TABLE III

TRAVELTIMES AND VELOCITIES FOR SEDIMENT FILLED BASINS

	Interval T	Velocity[*]
Unit I	.1000s	1.50 km/s
Unit II	.1323	1.89
Units III-V	.0896	2.01
Unit VIa	.1009	2.18
Unit VIb	-----	3.2

[*]Velocities are as given by Scientific Party, DSDP Leg 89

APPENDIC C

The following tables list the maximum free-air anomaly and minimum depth to seamounts in each of three seamounts groups: (1) the Emperors plus Midway; (2) the Musicians, and; (3) the Marshalls. A least squares line was fit to each of these groups of data and the results are shown in Figure 24. Only seamounts that were well surveyed were used. The locations of unnamed seamounts are given in latitude and longitude.

TABLE IV

LEAST SQUARES FITS

Emperors + Midway

Seamount Name	Max FAA (mgal)	Min Depth (m)
Midway	306 BA	0
Koko	257	293
48°50′N 168°20′E	140	2500
45°10′N 170°00′E	125	1400
Yomei	235	1000

	Max FAA (mgal)	Min Depth (m)
45.50°N 170.05°E	188	1493
Suiko	321	1090
Nintoku	335	1002
Jingu	277	812

Best fitting line, $y = -6.33x + 2602.11$, or $g_z = (2602.11m - z) / 6.33$

Correlation coefficient = -0.68

Musicians

Seamount Name	Max FAA (mgal)	Min Depth (m)
Paumakua	124	1880
Handel	76	2525
Kaluakalana	68	1827
Rimsky-Kor.	47	3627
Liszt	130	1600
Wagner	100	1950
Brahms	130	2125
Schubert	105	2600
Bizet	40	3700

Seamount Name	Max FAA (mgal)	Min Depth (m)
Tchaikovsky	85	2000
Berlin	25	3100
Hammerstein	85	2600
Mahler	70	2400
Stravinsky	45	2600
Donizetti	40	3900
Debussy	115	2200
Chopin	100	1850
Haydn	50	3600
Rapano Ridge	75	2500
Mendelssohn	140	1850

Best fitting line, $x = -0.04y + 179.39$, or $g_z = -0.04z + 179.39$

Correlation coefficient $= -0.79$

Marshalls

Seamount Name	Max FAA (mgal)	Min Depth (m)
6°40′N 172°25′E	70	2260
Van Valtier	153	1252
Harrie	175	1200
Majuro	230	0
Ailinglapalap	200	0

Best fitting line, $x = -0.06y + 222.16$, or $g_z = -0.06z + 222.16$

Correlation coefficient $= -0.95$

APPENDIX D

In Appendix C a least squares line was used to approximate the gravity–depth relationship in the Marshall Island group. Each of the seamounts in Figure 22 was then subtracted along a horizontal line from the Marshall least squares line. The resulting pseudo–isostatic values were plotted and contoured (Figure 25). The seamount names, numbers, and corrected values are listed below.

TABLE V

SEAMOUNT ISOSTATIC CORRECTION VALUES

Seamount Name	Correction (mgal)
Oroluk	22
10°25′N 156°45′E	59
11°10′N 156°50′E	82
12 15′N 156°20′E	65
Ita Mai Tai	122
14°00′N 157°40′E	115
Seascan	44
Zubov	100
16°05′N 163°05′E	−36

Seamount Name	Correction (mgal)
19°30′N 162°20′E	-27
21°30′N 159°30′E	48
Birdseye	17
19°15′N 164°50′E	70
Wake	47
M-3	9
Taongi	-3
Enewetak	-25
Ujelang	-28
9°50′N 160°55′E	20
Bikini	-53
Rongelap	-53
Wotho	-78
Ujae	-78
Kwajalein	-12
Ailinglapalap	-28
Jaluit	-28
Namorik	-3
Ebon	-28

Seamount Name	Correction (mgal)
Bikar	-53
Utirik	-53
Erikub	12
Maloelop	-28
Majuro	2
Van Valtier	10
6°40′N 172°25′E	-7
Mili	-31
Harrie	28
Makin	-28
Tarawa	-3
Sio	-42
MacDonald	-14
Harvey	-25
Niemeyer	-34
Allen	-34
Thomas	-14
MZP-6	126
MZP-3	115
Sylvania	36
Ponape	-28

Seamount Name	Correction (mgal)
$16°40'N$ $166°30'E$	-11
$15°30'N$ $153°10'E$	33
$19°45'N$ $153°20'E$	100
$21°20'N$ $153°10'E$	105
$24°15'N$ $152°15'E$	-10

APPENDIX E

In the model studies section five theoretical seamount shapes
were derived. These shapes were based upon the work of Jordan, et al.
(1983) which relates the height of the seamount (h) to the basal
radius (r). The ratio h/r was calculated for 63 seamounts in the
Pacific and are listed below. The mean ratio was used to construct
the seamount models shown in Figure 26.

TABLE VI

H/R AND R_2/R_1 RATIOS

G = guyot   C = conical   A = atoll   I = island   P = plateau

Seamount Name	Type	Min Depth (m)	Max Relief (m)	r (km)	h (km)	h/r
Seascan	G	1157	4343	35.70	3.66	.103
Van Valtier	G	1252	3248	23.88	2.78	.116
Ita Mai Tai	G	1402	4598	45.00	4.50	.100
Harrie	G	1200	3500	31.34	2.81	.090
19°15′N 164°50′E	G	1400	4000	41.96	3.73	.089
11°10′N 156°50′E	G	1550	4350	32.70	3.88	.119

Seamount Name	Type	Min Depth (m)	Max Relief (m)	r (km)	h (km)	h/r
10°25´N 156°45´E	G	1750	3750	23.68	2.93	.124
8°45´N 163°10´E	G	1098	3852	34.77	3.66	.105
14°25´N 165°50´E	G	967	4158	43.04	3.79	.088
16°05´N 163°05´E	G	1373	3927	38.23	3.38	.088
Rachmaninov	G	1814	3672	27.34	3.31	.121
Godard	G	2600	3300	17.36	2.59	.149
Suiko	G	1090	4810	58.08	4.77	.082
Nintoku	G	1002	4598	57.26	4.57	.080
Nagata	G	1559	3744	16.28	1.79	.110
Harvey	G	1200	4000	16.75	1.19	.071
MacDonald	G	1400	2600	24.48	2.76	.113
Niemeyer	G	1400	2800	17.60	1.65	.094
Thomas	G	1400	3800	15.92	1.69	.106
Zubov	C	1100	4550	19.60	3.13	.160
14°00´N 157°40´E	C	1250	4750	23.36	4.11	.176
12°15´N 156°20´E	C	1755	3395	27.15	3.86	.142
11°50´N 157°40´E	C	1830	3670	18.13	3.66	.202
16°40´N 166°30´E	C	2148	3152	23.05	3.16	.137
Paumakua	C	1880	2620	16.82	2.63	.156
Handel	C	2480	2770	13.13	2.64	.201
Kaluakalana	C	1827	2773	13.60	2.41	.177

Seamount Name	Type	Min Depth (m)	Max Relief (m)	r (km)	h (km)	h/r
Liszt	C	1600	4050	21.06	3.53	.168
MZP-6	C	1556	4294	26.90	3.93	.146
Tchaikovsky	C	2000	3500	11.28	2.87	.254
Berlin	C	3100	2750	7.01	2.15	.307
Mahler	C	2400	3500	15.75	2.20	.140
Debussy	C	2200	3400	15.65	3.72	.238
Haydn	C	3600	1350	14.90	2.96	.199
Finch	C	1000	3750	12.37	3.34	.270
Chautauqua	C	1785	2715	10.33	2.46	.238
Jasper	C	550	3470	15.95	3.66	.224
Jingu	C	812	5088	33.20	4.70	.142
Vityaz	C	841	5026	30.39	4.65	.153
19°45'N 153°20'E	C	1300	4400	21.79	3.91	.179
21°20'N 153°10'E	C	1100	4600	31.05	4.43	.143
Majuro	A	0	4450	27.55	3.66	.133
Enewetak	A	0	4575	36.30	3.66	.101
Bikini	A	0	4575	30.83	4.02	.130
Ailinglapalap	A	0	4488	36.73	4.02	.109
Taongi	A	0	5500	41.21	5.12	.124

Seamount Name	Type	Min Depth (m)	Max Relief (m)	r (km)	h (km)	h/r
Wotho	A	0	4575	22.79	4.02	.176
Maloelop	A	0	4488	40.26	4.02	.100
Mili	A	0	4488	48.80	4.02	.082
Jaluit	A	0	4400	44.20	4.02	.091
Ebon	A	0	4400	24.91	4.02	.161
Kusaie	A	0	4389	42.21	4.39	.104
Pearl & Hermes	A	0	4938	40.92	4.02	.098
Midway	A	0	5500	27.71	3.66	.132
22°40′N 161°00′W	A	0	4575	37.58	3.96	.105
Oroluk	A	0	4675	64.23	4.39	.068
Minto Reef	A	0	4755	31.60	5.12	.162
Truk	A	0	4389	68.59	4.39	.064
Johnston	A	0	4950	42.56	4.75	.112
Makin	A	0	4575	30.50	4.02	.132
Wake	I	0	5300	34.97	5.12	.146
Nauru	I	0	4000	18.52	4.02	.217
Ponape	I	0	4750	56.99	4.02	.071
Sio	P	1130	4420	121.33	3.26	.027

APPENDIX F

To see if there was a relationship between the age of the sea floor at the time a seamount erupts on it and the maximum FAA of that seamount, the edifice age, sea floor age, the max FAA, the Marshall least squares fit (Appendix C), and their errors had to be compiled. the resulting plot with the best dated seamount or island groups is shown in Figure 31.

TABLE VII

SEA FLOOR/SEAMOUNT FORMATION AGE VS. FAA - THEOR. LINE

Seamount Name	Max FAA (mgal)	Norm. Compen. (mgal)	Sea Floor Age (Ma)	Edifice Age (Ma)	Error Range (Ma)	Median (Ma)
Nagata	87	-37.9	98-108	78.7+/-10.6K	8.7-39.9	24.3
Maui	280	92.1	75-95	1.32+/-.04K	78.7-88.7	83.7
Lanai	250	62.1	75-95	1.28+/_.04K	78.7-88.7	83.7
Molokai	270	82.1	75-95	1.52-1.89	78.3-88.3	83.3
Oahu	310	122.1	75-95	2.6-3.7	76.9-86.9	81.9
Kauai	340	152.1	75-95	5.8+/-0.2K	74.2-84.2	79.2
Niihau	290	102.1	75-95	5.5+/-0.2K	ʼ74.5-84.5	79.5
Nihoa	285	97.1	75-95	7.2+/-0.3K	72.8-82.8	77.8

Seamount Name	Max FAA (mgal)	Norm. Compen. (mgal)	Sea Floor Age (Ma)	Edifice Age (Ma)	Error Range (Ma)	Median (Ma)
Laysan	290	102.1	105+/-5	19.9+/-0.3K	80.1-90.1	85.1
Pearl & Her.	285	97.1	111+/-5	20.6+/-0.5K	85.4-95.4	90.4
Midway	306	118.1	113+/-5	27.7+/-0.6K	80.3-90.3	85.3
Hawaii	330	142.1	75-95	0-.86+/-.05K	79.1-89.1	84.1
Tahiti	230	42.1	61+/-5	0.4-1.2 (?)	55.2-65.2	60.2
Moorea	215	27.1	61+/-5	1.5-1.6 (?)	54.5-64.5	59.5
Jasper	98	-67.7	22+/-5	----------	---------	----
Bermuda	355	167.1	108-118	33.5+/-2K	72.5-86.5	79.5
Koko	257	80.8	70-110	48.1+/-0.8K	21.9-61.9	41.9
Iceland	60	-127.9	0.0	0-4	0-4	2
Suiko	321	177.1	70-110	64.7+/-1.1K	5.3-45.3	25.3
Nintoku	335	187.6	70-110	56.2+/-0.6K	13.8-53.8	33.8
Jingu	277	121.9	70-110	55.4+/-0.9K	14.6-54.6	34.6
Enewetak	203	13.1	154+/-10	60.5+/-2.0K	86.2-109.0	97.6
Ponape	200	12.1	154+/-10	5-7K	136.0-156.0	146.0
Kosrae	250	62.1	147+/-5	1.3+/-0.1K	140.6-150.8	145.7
Truk	200	12.1	--------	8-14K	138.6-159.4	149.0
Lamont	200(?)	----	--------	86.6+/-3.7K	58.7-80.1	69.4
Diakakuji	140	-10.2	70-110	42.4+/-2.2K	27.5-67.7	47.6
Yuryaku	91	-85.2	70-110	42.8+/-1.6K	27.1-67.3	47.2
Kimmei	75	-73.0	70-110	39.4+/-1.2K	30.6-70.6	50.6

Seamount Name	Max FAA (mgal)	Norm. Compen. (mgal)	Sea Floor Age (Ma)	Edifice Age (Ma)	Error Range (Ma)	Median (Ma)
Ojin	225	78.8	70–110	55.2+/−0.7K	14.8–54.8	34.8
Galapagos	75–120	−157.9+/−15.8	6+/−2	1.11+/−.37	4.53–5.26	4.89
Rachmaninoff	75	−112.9	85+/−5	86.6+/−10.7K	0–14.1	7.1
Khachaturian	100	−87.9	85+/−5	66.8+/−2.6K	10.6–25.8	18.2
Atlantis	150	−37.9	113+/−5	95.2+/−6.8Ar	6.1–29.6	17.8
Cross	100	−87.9	85+/−5	84.4+/−5.3K	0–10.9	5.5
Great Meteor	250	62.1	80+/−5	11–16K (min)	59.0–74.0	66.5

APPENDIX H

The locations, free-air or Bouguer anomaly values, and depths of seamounts, atolls, and islands are given in the following table.

TABLE VIII

SEAMOUNT DATA TABLE

	LATITUDE	LONGITUDE	MAX. FAA or BA * (mgal)	MAX. AMPL (mgal)	MIN. DEPTH (m)	SEAFLR DEPTH (m)
LOCATION: MUSICIANS, MARSHALLS, MAPMAKERS						
Paumakua	24°50′N	157°05′W	124	133	1880	4500
Finch	17°32′N	157°35′W	123	127	1000	4750
Handel	27°26′N	159°53′W	76	87	2480	5250
Seascan	15°20′N	158°45′E	195	220	1157	5500
Birdseye	20°53′N	165°40′E	115	190	2392	5500
LOCATION: MUSICIANS, MARSHALLS, LINE, MID-PACS						
Kaluakalana	23°18′N	158°25′W	68	89	1827	4600
Rimsky-Korsakov	25°28′N	159°45′W	47	58	3627	5000
Van Valtier	7°20′N	172°20′E	153	164	1252	4500
Nagata	12°30′N	167°00′W	87	82	1559	5303
Sio	18°18′N	171°06′E	110	210	1130	5550

	LATITUDE	LONGITUDE	MAX. FAA or BA (mgal)	MAX. AMPL (mgal)	MIN. DEPTH (m)	SEAFLR DEPTH (m)
LOCATION: MARSHALLS, HAWAIIAN CHAIN						
Ita Mai Tai						
	13°00′N	156°45′E	255	322	1402	6100
Maui	20°42′N	156°06′W	280	405	----	5125
Kahoolawe	20°35′N	156°40′W	250	375	----	4400
Lanai	20°48′N	156°54′W	250	375	----	4400
Molokai	21°12′N	157°00′W	270	395	----	4400 SW; 4575 NE
LOCATION: LEEWARD ISLANDS, HAWAIIAN ISLANDS						
Oahu	21°30′N	158°00′W	310	385	----	4600
Kauai	22°00′N	159°30′W	340	390	----	4400
Niihau	21°54′N	160°12′W	290	340	----	4575
Nihoa	23°06′N	161°54′W	285	310	----	4700
LOCATION: LEEWARD ISLANDS, HAWAIIAN ISLANDS						
Laysan	25°48′N	171°42′W	290	340	----	4575 S; 4950 N
Lisianski	26°00′N	174°48′W	314	339	----	4950
Pearl & Hermes Reef						
	27°54′N	175°48′W	285	310	----	4750 SW; 5125 NE

	LATITUDE	LONGITUDE	MAX. FAA or BA (mgal)	MAX. AMPL (mgal)	MIN. DEPTH (m)	SEAFLR DEPTH (m)
Midway	$28°18'N$	$177°18'W$	306	356	----	5500
Hawaii	$19°30'N$	$155°30'W$	330	430	----	5125
Johnston	$16°45'N$	$169°30'W$	251	301	----	4950

LOCATION: SAMOA, SOCIETY ISLANDS, MANUA ISLANDS

	LATITUDE	LONGITUDE	MAX. FAA or BA (mgal)	MAX. AMPL (mgal)	MIN. DEPTH (m)	SEAFLR DEPTH (m)
Tutuila	$14°20'S$	$170°40'W$	290	538	----	----
Ofu & Olosega	$14°10'S$	$169°40'W$	310	558	----	----
Tau	$14°15'S$	$169°30'W$	290	538	----	----
Tahiti	$17°40'S$	$149°30'W$	230	305	----	----
Moorea	$17°30'S$	$149°50'W$	215	290	----	----

LOCATION: MISCELLANEOUS

	LATITUDE	LONGITUDE	MAX. FAA or BA (mgal)	MAX. AMPL (mgal)	MIN. DEPTH (m)	SEAFLR DEPTH (m)
Jasper	$30°32'N$	$122°42'W$	98	128	550	4020
Chautauqua	$21°10'N$	$162°40'W$	40	60	1785	4500
Great Meteor	$30°00'N$	$28°30'W$	250	290	250	4800
Bermuda	$32°20'N$	$64°45'W$	355	395	----	5000
Koko	$35°15'N$	$171°35'E$	257	335	293	5250
Unnamed	$35°00'N$	$46°00'W$	30	60	2750	4500

	LATITUDE	LONGITUDE	MAX. FAA or BA (mgal)	MAX. AMPL (mgal)	MIN. DEPTH (m)	SEAFLR DEPTH (m)
Iceland	65°00′N	18°00′W	60	70	----	1400
Unnamed	48°50′N	168°20′E	140	240	2500±200	6150
Unnamed	45°10′N	170°00′E	125	240	1400±100	5900
Yomei	42°18′N	170°24′E	235	315	1000	5700
LOCATION:	MID-PACIFIC MOUNTAINS					
M-3	12°14′N	173°13′E	130	140	1600	5700
Harvey	17°50′N	172°40′E	120	140	1200	5200
MacDonald	19°10′N	173°20′E	120	200	1400	4000
Niemeyer	18°05′N	173°35′E	100	120	1400	4200
LOCATION:	W. MARSHALLS, MID-PACS					
Thomas	17°20′N	173°55′E	120	160	1400	5200
Harrie	5°40′N	172°20′E	175	215	1200	4700
Unnamed	19°15′N	164°50′E	205	240	1400	5400
Unnamed	11°10′N	156°50′E	205	240	1550	5900
Unnamed	10°25′N	156°45′E	170	190	1750	5500
LOCATION:	EMPERORS, MARSHALLS					
Unnamed	45.4967°N	170.0523°E	188	270	1493	5800
Suiko	44.5499°N	170.2770°E	321	435	1090	5900

	LATITUDE	LONGITUDE	MAX. FAA or BA (mgal)	MAX. AMPL (mgal)	MIN. DEPTH (m)	SEAFLR DEPTH (m)
Nintoku	41.0223°N	170.5910°E	335	418	1002	5600
Jingu	38.7926°N	171.1445°E	277	350	812	5900

LOCATION: WEST MARSHALLS, MUSICIANS

	LATITUDE	LONGITUDE	MAX. FAA or BA (mgal)	MAX. AMPL (mgal)	MIN. DEPTH (m)	SEAFLR DEPTH (m)
Zubov	15°40′N	160°00′E	255	280	1100	5700 NE; 5600 SW
Unnamed	14°00′N	157°40′E	260	295	1250	6000
Unnamed	12°15′N	156°20′E	175	190	1755	5150
Unnamed	6°40′N	172°25′E	70	105	2260	4700
Liszt	28°59′N	162°00′W	130	150	1600	5650

LOCATION: MUSICIANS

	LATITUDE	LONGITUDE	MAX. FAA or BA (mgal)	MAX. AMPL (mgal)	MIN. DEPTH (m)	SEAFLR DEPTH (m)
Wagner	30°46′N	162°54′W	100	135	1950	5950
Brahms	31°09′N	162°19′W	130	145	2125	5700
Schubert	31°56′N	162°09′W	105 '	125	2600	5800
Bizet	32°16′N	161°38′W	40	70	3700	5950
Tchaikovsky	29°23′N	162°05′W	85	85	2000	5500
Berlin	32°51′N	166°00′W	25	35	3100	5850
Hammerstein	32°28′N	165°46′W	85	110	2600	5850
Mahler	31°46′N	164°58′W	70	95	2400	5900

	LATITUDE	LONGITUDE	MAX. FAA or BA (mgal)	MAX. AMPL (mgal)	MIN. DEPTH (m)	SEAFLR DEPTH (m)
Nintoku	41.0223°N	170.5910°E	335	418	1002	5600
Jingu	38.7926°N	171.1445°E	277	350	812	5900
LOCATION:	WEST MARSHALLS, MUSICIANS					
Zubov	15°40´N	160°00´E	255	280	1100	5700 NE; 5600 SW
Unnamed	14°00´N	157°40´E	260	295	1250	6000
Unnamed	12°15´N	156°20´E	175	190	1755	5150
Unnamed	6°40´N	172°25´E	70	105	2260	4700
Liszt	28°59´N	162°00´W	130	150	1600	5650
LOCATION:	MUSICIANS					
Wagner	30°46´N	162°54´W	100	135	1950	5950
Brahms	31°09´N	162°19´W	130	145	2125	5700
Schubert	31°56´N	162°09´W	105	125	2600	5800
Bizet	32°16´N	161°38´W	40	70	3700	5950
Tchaikovsky	29°23´N	162°05´W	85	85	2000	5500
Berlin	32°51´N	166°00´W	25	35	3100	5850
Hammerstein	32°28´N	165°46´W	85	110	2600	5850
Mahler	31°46´N	164°58´W	70	95	2400	5900

	LATITUDE	LONGITUDE	MAX. FAA or BA (mgal)	MAX. AMPL (mgal)	MIN. DEPTH (m)	SEAFLR DEPTH (m)
Stravinsky	31°29´N	164°36´W	45	60	2600	5900
Donizetti	32°20´N	160°00´W	40	65	3900	5900
Debussy	30°18´N	162°05´W	115	130	2200	5600
Chopin	26°08´N	162°03´W	100	100	1850	5250 N; 5000 S
Haydn	26°40´N	161°12´W	50	55	3600	4950
Rapano Ridge 26°40´N		159°00´W	75	85	2500	5400

LOCATION: MUSICIANS, LEEWARD ISLES

	LATITUDE	LONGITUDE	MAX. FAA or BA	MAX. AMPL	MIN. DEPTH	SEAFLR DEPTH
Mendelssohn 25°10´N		161°39´W	100	100	1850	5050
Unnamed	22°40´N	161°00´W	50	75	---	4575
French Frigate Shoals 23°45´N		166°10´W	275	---	---	4750
Gardner Pinnacles 25°00´N		168°00´W	175	228	---	4575
Unnamed	25°40´n	169°30´W	200	253	---	4575

LOCATION: LEEWARD ISLES, MARSHALLS, CAROLINES

	LATITUDE	LONGITUDE	MAX. FAA or BA	MAX. AMPL	MIN. DEPTH	SEAFLR DEPTH
Maro Reef	25°30´N	171°00´W	133	187	---	4575
Unnamed	8°45´N	163°10´E	165	230	1098	4950
Enewetak	11°30´N	162°20´E	203	268	---	4575

	LATITUDE	LONGITUDE	MAX. FAA or BA (mgal)	MAX. AMPL (mgal)	MIN. DEPTH (m)	SEAFLR DEPTH (m)
Bikini	11°35´N	165°25´E	175	175	---	4575
Oroluk	7°30´N	155°20´E	250	265	---	4400 SW; 4950 NE
LOCATION: MARSHALLS						
Rongelap	11°15´N	166°50´E	175	175	---	4400
Kwajalein	9°10´N	167°25´E	216	216	---	4400 N; 4950 SW
Ailinglapalap	7°25´N	168°50´E	200	200	---	4025 NE; 4950 SW
Bikar	12°15´N	170°05´E	175	200	---	4575 W; 4950 E
Taongi	14°35´N	168°55´E	225	232	---	5500
Ujelang	9°50´N	160°55´E	200	200	---	4025 NE; 4750 SW
Wotho	10°05´N	166°00´E	150	150	---	4575
Ujae	9°05´N	165°35´E	150	150	---	4950 SW; 4400 NE
Utirik	11°10´N	169°45´E	175	200	---	4575
Erikub	9°10´N	170°00´E	240	240	---	4400
Maloelop	8°45´N	171°05´E	200	200	---	4025 W; 4950 E

	LATITUDE	LONGITUDE	MAX. FAA or BA (mgal)	MAX. AMPL (mgal)	MIN. DEPTH (m)	SEAFLR DEPTH (m)
LOCATION:	MARSHALLS, GILBERTS					
Mili	6°10'N	172°00'E	197	222	----	4400 W; 4575 E
Jaluit	6°00'N	169°10'E	200	200	----	4400
Namorik	5°40'N	168°10'E	225	250	----	4575
Ebon	4°40'N	168°45'E	200	225	----	4400
Makin	3°10'N	172°50'E	200	235	----	4400 W; 4750 E
Tarawa	1°30'N	172°55'E	225	225	----	4400
Wake	19°15'N	166°40'E	275	275	----	5300
Unnamed	16°05'N	163°05'E	100	100	1373	5300
Unnamed	19°30'N	162°20'E	125	125	1136	5125
LOCATION:	MARSHALLS, KK81062604					
Unnamed	21°30'N	159°30'E	200	250	1151	5500
853	11°45'– 13°15'N	147°15'– 148°30'E	170	170	1561	5675
MZP-6	13°00'– 14°30'N	155°30'– 157°30'E	250	320	1556	5850
MZP-3	13°00' 15°00'N	157°30'– 161°00'E	255	295	1373	5500
Sylvania	11°58'N	165°00'E	180	190	1263	4950

	LATITUDE	LONGITUDE	MAX. FAA or BA (mgal)	MAX. AMPL (mgal)	MIN. DEPTH (m)	SEAFLR DEPTH (m)
LOCATION:	CAROLINES, MARSHALLS, MAGELLANS					
Ponape	6°50'N	158°15'E	200	200	----	4750
Unnamed	16°40'N	166°30 E	75	105	2148	5300
Unnamed	15°30'N	153°10'E	65	130	2928	5300
LOCATION:	MAGELLANS					
Unnamed	19°45'N	153°20'E	240	265	1300	5700
Unnamed	21°20'N	153°10'E	260	275	1100	5700
Unnamed	24°15'N	152°15'E	100	125	1750	5300
Nauru	0°16'S	166°55'	175	175	----	4000
LOCATION:	MID-PACS, CAROLINES					
Vityaz	13°30'N	173°15'W	?	?	841	5485
Kusaie	5°10'N	163°oo'E	250	250	----	4570
Minto Reef	8°08'N	154°15'E	250	225	----	5120
Truk	7°25'N	151°45'E	200	200	----	4390
Wilde	21°12'N	163°24'E	----	----	1244	5120
LOCATION:	S. CHINA SEA, MARCUS RIDGE, EMPERORS					
Miami	21°42'N	116°54'E	----	----	13	180
Lamont	21°30'N	159°30'E	----	----	1150	5485

	LATITUDE	LONGITUDE	MAX. FAA or BA (mgal)	MAX. AMPL (mgal)	MIN. DEPTH (m)	SEAFLR DEPTH (m)
Scripps	23°54′N	159°30′E	---	---	1298	5485
Kammu	32°06′N	172°48′E	---	---	320	5120
Diakakuji	32°06′N	172°18′E	---	---	933	5120
LOCATION:	EMPERORS, E. PAC					
Yuryaku	32.7°N	172.1°E	91	---	293	5120
Kimmei	33.7°N	171.6°E	75	---	988	5485
Ojin	37.8°N	170.4°E	225	---	1033	5395
Meiji	53.0°N	165.0°E	---	---	2925	5120
Henderson	25.333°N	119.5°W	---	---	535	3839
LOCATION:	E. PAC, MUSICIANS					
Horizon	19.283°N	169.000°W	---	---	1442	5000
Li	6.2°N	186.0°W	---	---	----	----
Khatchaturian	28.138°N	162.278°W	---	---	----	----
Rachmanioff	29.555°N	163.372°W	---	---	----	----
Wentworth	28.900°N	177.867°W	---	---	----	----
LOCATION:	HAW. RIDGE					
Necker	23.802°N	164.423°W	---	---	----	----

	LATITUDE	LONGITUDE	MAX. FAA or BA (mgal)	MAX. AMPL (mgal)	MIN. DEPTH (m)	SEAFLR DEPTH (m)
L2	----	----	---	---	----	----
L3	----	----	---	---	----	----
Moonless	----	----	---	---	----	----
HD1	18.3°N	161.8°W	---	---	----	----

LOCATION: HAW. RIDGE, JAPAN LINE IS., MISC.

	LATITUDE	LONGITUDE	MAX. FAA or BA (mgal)	MAX. AMPL (mgal)	MIN. DEPTH (m)	SEAFLR DEPTH (m)
Unnamed	26.5°N	177.8°W	---	---	----	----
Sisoev	40/9°N	144.9°E	---	---	----	----
Ryotu	38.0°N	146.0°E	---	---	----	----
Kapsitotwa	12.0°N	165.8°W	---	---	----	----
Stanley	8.2°N	161.9°W	----	---	----	----
Atlantis	38.4°N	63.3°W	150	---	1000	4575
Cross	18.4°N	158.1°W	100	---	340	4600

*max FAA for seamounts, max BA (2.3 g/cm^3) for islands

BIBLIOGRAPHY

Batiza, R., Abundances, distribution and sizes of volcanoes in the Pacific Ocean and implications for the origin of non-hotspot volcanoes, E.P.S.L., 60, 195-206, 1982.

Gregory, A. E., III, and L. W. Kroenke, Reef development in a mid-oceanic island; reflection profiling studies of the 500-meter shelf south of Oahu, AAPG Bull., 66, 843-859, 1982.

Furumoto, A. S., J. F. Campbell, and D. M. Hussong, Seismic studies of subsurface structure in the Ewa coastal plain, Oahu, Hawaii, Pacific Sci., 24, 529-542, 1970.

Heezen, B. C. et al., Tertiary pelagic ooze on Ita Maitai guyot; equatorial Pacific: DSDP sites 200 and 201, in Initial Reports of the Deep Sea Drilling Project, vol. 20, edited by B. C. Heezen and I. D. MacGregor, pp. 87-96, U.S. Government Printing Office, Washington, D.C., 1973.

Heezen, B. C., MacGregor, I. D., Oolitic limestone on the Ita Maitai Guyot, Equatorial Pacific: DSDP Site 202, in Initial Reports of the Deep Sea Drilling Project, vol. 20, edited by B. C. Heezen and I. D. MacGregor, pp. 97-102, U.S. Government Printing Office, Washington, D.C., 1973.

Hesse, R., Diagenesis of a seamount oolite from the west Pacific, Leg 20, DSDP, in Initial Reports of the Deep Sea Drilling Project, vol. 20, edited by B. C. Heezen et al., pp. 363-387, U.S. Government Printing Office, Washington, D.C., 1973.

Hilde, T. W. C., N. Isezaki, and J. M. Wageman, Mesozoic sea-floor spreading in the North Pacific, in The Geophysics of the Pacific Ocean Basin and its Margin, Geophys. Monogr. Ser., vol. 19, edited by G. H. Sutton, M. H. Manghnani, and R. Moberly, pp. 205-226, Amer. Geophys. Union, Washington, D. C., 1976.

Hilde, T. W. C., S. Uyeda, and L. Kroenke, Evolution of the western Pacific and its margin, Tectonophysics, 38, 145-165, 1977.

Jones, E. J. W., Determination of sedimentary velocities using expendable sonobuoys at DSDP Leg 20 drilling sites, northwest Pacific, in Initial Reports of the Deep Sea Drilling Project, vol. 20, edited by B. C. Heezen and I. D. MacGregor, pp. 625-642, U. S. Government Printing Office, Washington, D. C., 1973.

Jordan, T. H., H. W. Menard, and D. K. Smith, Density and size distribution of seamounts in the eastern Pacific inferred from wide-beam sounding data, J. Geophys. Res., 88, 10508-10518, 1983.

Kellogg, J. N., and I. J. Ogujiofor, Gravity field analysis of Sio Guyot: An isostatically compensated seamount in the Mid-Pacific Mountains, Geo-Marine Letters, 5, 91-97, 1985.

Kellogg, J. N., B. S. Wedgeworth, and I. J. Ogujiofor, Invited Paper, Three-dimensional modeling of the gravity fields of seamounts, Abst., SEG/USN Tech. Symposium on 3-Dimensional Marine Data Collection, Processing, Interpretation, and Presentation, NSTL, Miss., p. 9, 1984.

Kroenke, L. W., Geology of the Ontong Java Plateau, Hawaii Institute of Geophysics Report 72-5, Honolulu, Hawaii, pp. 1-119, 1972.

Larson, R. L., Late Jurassic and Early Cretaceous evolution of the western central Pacific Ocean, J. Geomag. Geoelectr. 28, 219-236, 1976.

Larson, R. L., and C. G. Chase, Late Mesozoic evolution of the western Pacific Ocean, GSA Bull., 83, 3627-3644, 1972.

Le Pichon, X., and M. Talwani, Crustal structure of the mid-ocean ridges; 1, Seismic refraction measurements, J. Geophys. Res., 70, 319-339, 1965.

Lonsdale, P., and F. N. Spiess, A pair of young cratered volcanoes on the East Pacific Rise, J. of Geology, 87, 157-173, 1979.

Menard, H. W., Marine Geology of the Pacific, 271 pp., McGraw-Hill, New York, 1964.

Menard, H. W., Darwin reprise, J. Geophys. Res., 89, 9960-9968, 1984.

Ozima, M., M. Honda, and K. Saito, ^{40}Ar-^{39}Ar ages of guyots in the western Pacific and discussion of their evolution, Geophys. J. Roy. Astr. Soc., 51, 475-485, 1977.

Plouff, D., Gravity and magnetic fields of polygonal prisms and application to magnetic terrain corrections, Geophysics, 41, 727-741, 1976.

Press, F., Seismic velocities, in Handbook of Physical Constants, edited by S. P. Clark, Jr., pp. 202-203, Geol. Soc. America Mem. 97, 1966.

Richards, M. L., V. Vacquier, and G. D. van Voorhis, Calculation of the magnetization of uplifts from combining topographic and magnetic surveys, Geophysics, 32, 678-707, 1967.

Rose, J. C., and B. R. Bowman, The effect of seamounts and other bottom topography on marine gravity anomalies, in _Proceedings of the International Symposium on Applications of Marine Geodesy_, pp. 381-396, Mar. Tech. Soa., Washington, D. C., 1974.

Sager, W. W., G. T. Davis, B. H. Keating, and J. A. Philpotts, A geophysical and geologic study of Nagata Seamount, northern Line Islands, _J. Geomag. Geoelectr., 34_, 283-305, 1982.

Schimke, G. R., and C. G. Bufe, Geophysical description of a Pacific Ocean seamount, _J. Geophys. Res., 73_, 559-569, 1968.

Schlanger, S. O., and I. Premoli-Silva, Tectonic, volcanic and paleographic implications of redeposited reef faunas of late Cretaceous and Tertiary age from the Nauru Basin and Line Islands, in _Initial Reports of the Deep Sea Drilling Project_, vol. 61, edited by R. L. Larson et al., pp. 817-827, U. S. Government Printing Office, Washington, D. C., 1981.

Scientific Party, Leg 89, Leg 89 drills Cretaceous volcanics, _Geotimes, 28_, 17-20, 1983.

Shipley, T. H., J. M. Whitman, F. K. Duennebier, and L. D. Petersen, Seismic stratigraphy and sedimentary history of the East Mariana Basin, western Pacific, _Earth Planet. Sci. Lett., 64_, 257-275, 1983.

Stoeser, D. B., Igneous rocks from Leg 30 of the Deep Sea Drilling Project, in _Initial Reports of the Deep Sea Drilling Project, vol. 30_, edited by J. E. Andrews, G. Peckham, et al., pp. 401-414, U. S. Government Printing Office, Washington, D. C., 1975.

Strange, W. E., G. P. Woollard, and J. C. Rose, An analysis of the gravity field over the Hawaiian Islands in terms of crustal structure, Pac. Sci., 19, 381-389, 1965.

Udintsev, G. B. et al., Seamounts of the Pacific Ocean, in Volcanoes and Tectonosphere, edited by H. Aoke and S. Iizuka, pp. 7-33, Tokai University Press, Shimizu, Japan, 1976.

Watts, A. B., U. S. ten Brink, P. Buhl, and T. M. Brocher, A multichannel seismic study of lithospheric flexure across the Hawaiian-Emperor seamount chain, Nature, 315, 105-111, 1985.

Woollard, G. P., The relation of gravity anomalies to surface elevation, crustal structure and geology, Research Report Series No. 62-9, pp., Aeronautical Chart and Information Center, United States Air Force, St. Louis, Missouri, 1962.

DATE DUE

FEB 21 1986		
APR 1 1986		
1 16 87		